METHODS

Zircon for U–Pb and U–Th geochronology was separated from ~0.2–2 kg crushed and sized samples using heavy liquids, mounted on glass and cast in 25 mm diameter epoxy plugs along with R33 standard zircon grains, ground to expose grains in cross section, polished, and imaged with reflected light and SEM cathodoluminescence (CL). Inclusions exposed on polished surfaces of zircon crystals were located with SEM backscattered-electron imaging and identified by their x-ray energy spectra. Spots were selected for analysis with the Sensitive High-Resolution Ion Microprobe with Reverse Geometry (SHRIMP-RG) at the Stanford–USGS laboratory at Stanford University on the basis of internal zoning revealed in CL. During the mass scans for U–Pb geochronology concentrations of U, Th, Hf, La, Ce, Nd, Sm, Eu, Gd, Dy, Er, and Yb also were measured.

Prior to analysis with the Sensitive High-Resolution Ion Microprobe with Reverse Geometry (SHRIMP-RG) at the Stanford–USGS laboratory at Stanford University, the epoxy plug was washed with saturated EDTA and dilute HCl solutions, rinsed with distilled water, dried in a vacuum oven, and coated with 100 nm of gold. A primary beam of O_2^- with intensities of ~6 nA for U–Pb analyses and ~10-15 nA for ^{238}U–^{230}Th analyses was focused into a 20–30 micrometer spot to generate secondary ions. The primary beam was rastered for 90–120 seconds over the analysis area before data were collected. For U–Pb geochronology, counts for secondary ions were collected sequentially with a single ETP electron multiplier on the following peaks: $^{90}Zr_2{}^{16}O^+$ (2 s), $^{204}Pb^+$ (8 s), background (8 s at 0.050 mass units above $^{204}Pb^+$), $^{206}Pb^+$ (30 s), ^{207}Pb+ (20 s), $^{208}Pb^+$ (8 s), $^{238}U^+$ (6 s), $^{232}Th^{16}O^+$ (3 s), $^{238}U^{16}O^+$ (3 s), $^{139}La^+$ (2 s), $^{140}Ce^+$ (1 s each for rest),

$^{89}Y^+$, $^{146}Nd^+$, $^{147}Sm^+$, $^{153}Eu^+$, $^{155}Gd^+$, $^{163}Dy^{16}O^+$, $^{166}Er^{16}O^+$, $^{172}Yb^{16}O^+$, $^{180}Hf^{16}O^+$, and $^{238}U^{16}O_2^+$; measurements were made at mass resolution of ~8000–9500 (10% peak height), which resolves all interfering atomic species. For U–Th analyses, secondary ion intensity was measured over seven scans for $^{90}Zr_2^{16}O^+$ (2 s), $^{180}Hf^{16}O^+$ (2 s), $^{238}U^{16}O^+$ (6 s), $^{230}Th^{16}O^+$ (60 s), background at 0.05 amu below $^{230}Th^{16}O^+$ (60 s), $^{232}Th^{16}O^+$ (3 s), $^{235}U^{16}O^+$ (6 s), $^{238}U^{16}O^+$ (3 s) and $^{232}Th^{12}C^+$ at ~244 amu (10 s) to monitor for a potential isobaric interference at mass 246 due to partial overlap of the primary beam on surrounding epoxy (see Schmitt, 2006). Relative ionization between U and Th was constrained by repeated intra-session analysis of standards R33 (419 Ma, quartz diorite of Braintree complex, Vermont, Black et al., 2004) and homogenous in-house MAD-green zircon from Madagascar (Barth and Wooden, 2010), both of which are sufficiently old (ca. 419 and 555 Ma, respectively) to have ^{238}U and ^{230}Th in secular equilibrium. Concentration data for zircons were standardized against MAD-green zircon relative to intensities for $^{90}Zr_2^{16}O^+$; U–Pb ages were calculated by calibration against zircon standard R33 which was analyzed repeatedly throughout the duration of the analytical sessions. Data reduction followed the methods described by Williams (1997) and Ireland and Williams (2003), and used the Squid 1 and Isoplot programs of Ken Ludwig (Ludwig 2001, 2003).

Whole rock major- and trace-element concentrations were determined by GeoAnalytical Laboratories (Washington State University) on powders of the three largest samples (19B, 24B, 24C); comparable data for sample 5i appear in Nye et al. (1994, table 4). Minerals and glass in the six samples were analyzed with a JEOL 8900 electron microprobe at the USGS in Menlo Park, California.

FIGURES

Figure DR1. Transmitted light images of polished thin sections of xenoliths from Redoubt Volcano. Images are approximately 2.4 x 3.6 cm. A: Crystal-rich andesite 19B. Plagioclase in gabbroic clusters in lower center region is $An_{83–92}$ zoned to rims as low as An_{46}; large sieved plagioclase is mainly $An_{48–59}$ with rims of similar composition; two plagioclase inclusions in hornblende oikocryst near upper center are An_{88} and An_{64} zoned to An_{57} and An_{51}, respectively. Hornblende oikocryst is identical in composition to those in gabbro 22. Note textural heterogeneity of sample and doublet of olivine xenocrysts (Fo_{81}, 900 ppm Ni) with opaque mantle in right center. B: Gabbro 22. Plagioclase cores are $An_{79–89}$, rims are $An_{59–63}$, and inclusions in hornblende oikocrysts are $An_{56–85}$ zoned to $An_{55–70}$. C: Gabbro 24B. Typical plagioclase cores are $An_{75–79}$, rims $An_{55–58}$. D: Gabbro 21B. Typical plagioclase is $An_{94–95}$, with rims $An_{47–68}$. Olivine, enclosed in pyroxene, is $Fo_{75–79}$, ~300 ppm Ni. E: Gabbro 24C. Typical plagioclase cores are $An_{77–84}$, rims $An_{55–76}$. F: Gabbro 5i. Plagioclase cores are $An_{79–85}$ with many being $An_{80–81}$; rims are $An_{45–53}$.

Figure DR2. Concordia diagrams for SHRIMP-RG zircon U–Pb data. Uncertainties for error ellipses are ±2σ. Numbers by blue concordia curves are ages in Ma. Numbers adjacent to error ellipses identify specific spot analyses. A: Crystal-rich andesite 19B. B: Gabbro 22. C: Gabbro 24B. D: Gabbro 21B. E: Gabbro 24C. F: Gabbro 5i.

Figure DR3. Whole rock compositions of xenoliths and crystal-rich andesite from Redoubt Volcano. A: Elemental abundances normalized to primitive mantle values (Sun and McDonough, 1989). B: Rare earth element abundances normalized to chondrite values (Sun and McDonough, 1989).

Figure DR4. Cathodoluminescence images of zircons from xenoliths from Redoubt Volcano. Images of polished grain mounts were obtained with a JEOL scanning electron microscope. Sample number appears at top of image (e.g., 08RDCRB019B). All CL images are shown, including those for which no zircons were analyzed. Numbers by individual zircons identify analyses, e.g., 72.1 is zircon 72, analysis spot 1 in the sample. Numbers with uncertainties listed, e.g., 1861±8, are $^{238}U/^{206}Pb$ (<1000 Ma) or $^{207}Pb/^{206}Pb$ (≥1000 Ma) ages in Ma; uncertainties are ±1σ (D indicates analysis was >10% discordant). For two grains (08RDCRB019B zircon 62 and 90CNR05i zircon 1), ^{238}U–^{230}Th disequilibrium model ages are given; these are identified by units of ka. Uranium concentrations are given in separate CL images of low-U zircons.

Figure DR5. Concentrations of U and Hf (ppm) and Ce/Ce* ratios in zircon obtained during SHRIMP-RG U–Pb geochronology analyses. Symbols indicate age groups for nominal ages of analysis spots for all six samples plotted together. Note largely separate groups for 1800–1900 Ma and 280–350 Ma points. A: U vs. Hf. B: Ce/Ce* vs. Hf.

Figure DR6. Concentration ratios Yb/Gd vs. Th/U in zircon obtained during SHRIMP-RG U–Pb geochronology analyses. Symbols indicate age groups for nominal ages of analysis spots for all six samples plotted together. Note coherent trend in 1800–1900 Ma data and clustering of most 280–350 Ma points.

Figure DR7. Concentration ratio U/Ce vs. Th (ppm) in zircon obtained during SHRIMP-RG U–Pb geochronology analyses. Symbols indicate age groups for nominal ages of analysis spots for all six samples plotted together. Gray lines give reference U/Ce:Th ratios. Non-igneous zircon plots at U/Ce>2xTh. Note separation into two clusters for majority of 1800–1900 Ma and 280–350 Ma points. Spot analyzes with U/Ce >2 likely represent zircon that precipitated from aqueous fluid.

Figure DR8. Concentrations of REE in zircon obtained during SHRIMP-RG U–Pb geochronology analyses normalized to those in chondritic meteorites (Korotev, 1996). Values for Pr calculated on the basis of those for La and Nd. Symbols indicate age groups for nominal ages of analysis spots. A: Crystal-rich andesite 19B. B: Gabbro 22. C: Gabbro 24B. D: Gabbro 21B. E: Gabbro 24C. F: Gabbro 5i.

TABLES

Table DR1. Sample numbers and localities for xenoliths from Redoubt Volcano.

Table DR2. Chemical analyses of xenoliths from Redoubt Volcano.

Table DR3. Electron microprobe analyses of minerals and glass in xenoliths from Redoubt Volcano.

Table DR4. SHRIMP-RG U–Pb geochronology data and calculated ages for zircon from xenoliths from Redoubt Volcano.

Table DR5. SHRIMP-RG U–Th geochronology data and calculated ages for zircon from xenoliths from Redoubt Volcano.

Table DR6. SHRIMP-RG trace element concentrations and ratios for zircon from xenoliths from Redoubt Volcano.

REFERENCES CITED

Barth, A.P., and Wooden, J.L., 2010, Coupled elemental and isotopic analyses of polygenetic zircons from granitic rocks by ion microprobe, with implications for melt evolution and the sources of granitic magmas: Chemical Geology, v. 277, p. 149–159.

Cheng, H., Edwards, R.L., Hoff, J., Gallup, C.D., Richards, D.A., and Asmerom, Y., 2000, The half-lives of uranium-234 and thorium-230: Chemical Geology, v. 169, p. 17–33.

Korotev, R.L., 1996, A self-consistent compilation of elemental concentration data for 93 geochemical reference samples: Geostandards Newsletter, v. 20, p. 217–245.

Sano, Y., Terada, K., and Fukuoka, T., 2002, High mass resolution ion microprobe analysis of rare earth elements in silicate glass, apatite and zircon: lack of matrix dependency: Chemical Geology, v. 184, p. 217–230.

Sun, S.-s., and McDonough, W.F., 1989, Chemical and isotopic systematics of oceanic basalts: implications for mantle composition and processes, *in* Saunders, A.D., and Norry, M.J., eds., Magmatism in the Ocean Basins, The Geological Society, London, Special Publication 42, p. 313–345.

Swanson, S.E., Nye, C.J., Miller, T.P, and Avery, V.F., 1994, Geochemistry of the 1989–1990 eruption of Redoubt Volcano: Part II. Evidence from mineral and glass chemistry: Journal of Volcanology and Geothermal Research, v. 62, p. 453–468.

Till, A.B., Yount, M.E., and Bevier, M.L., 1994, The geologic history of Redoubt Volcano, Alaska: Journal of Volcanology and Geothermal Research, v. 62, p. 11–30.

Wilson, C.J.N., Charlier, B.L.A., Rowland, J.V., and Browne, P.R.L., 2010, U-Pb dating of zircon in subsurface, hydrothermally altered pyroclastic deposits and implications for subsidence in a magmatically active rift: Taupo Volcanic Zone, New Zealand: Journal of Volcanology and Geothermal research, v. 191, p. 69-78.

Figure DR1. Transmitted light images of polished thin sections of xenoliths from Redoubt Volcano. Images are approximately 2.4 x 3.6 cm. A: Crystal-rich andesite 19B. Plagioclase in gabbroic clusters in lower center region is An_{83-92} zoned to rims as low as An_{46}; large sieved plagioclase is mainly An_{48-59} with rims of similar composition; two plagioclase inclusions in hornblende oikocryst near upper center are An_{88} and An_{64} zoned to An_{57} and An_{51}, respectively. Hornblende oikocryst is identical in composition to those in gabbro 22. Note textural heterogeneity of sample and doublet of olivine xenocrysts (Fo_{81}, 900 ppm Ni) with opaque mantle in right center. B: Gabbro 22. Plagioclase cores are An_{79-89}, rims are An_{59-63}, and inclusions in hornblende oikocrysts are An_{56-85} zoned to An_{55-70}. C: Gabbro 24B. Typical plagioclase cores are An_{75-79}, rims An_{55-58}. D: Gabbro 21B. Typical plagioclase is An_{94-95}, with rims An_{47-68}. Olivine, enclosed in pyroxene, is Fo_{75-79}, ~300 ppm Ni. E: Gabbro 24C. Typical plagioclase cores are An_{77-84}, rims An_{55-76}. F: Gabbro 5i. Plagioclase cores are An_{79-85} with many being An_{80-81}; rims are An_{45-53}.

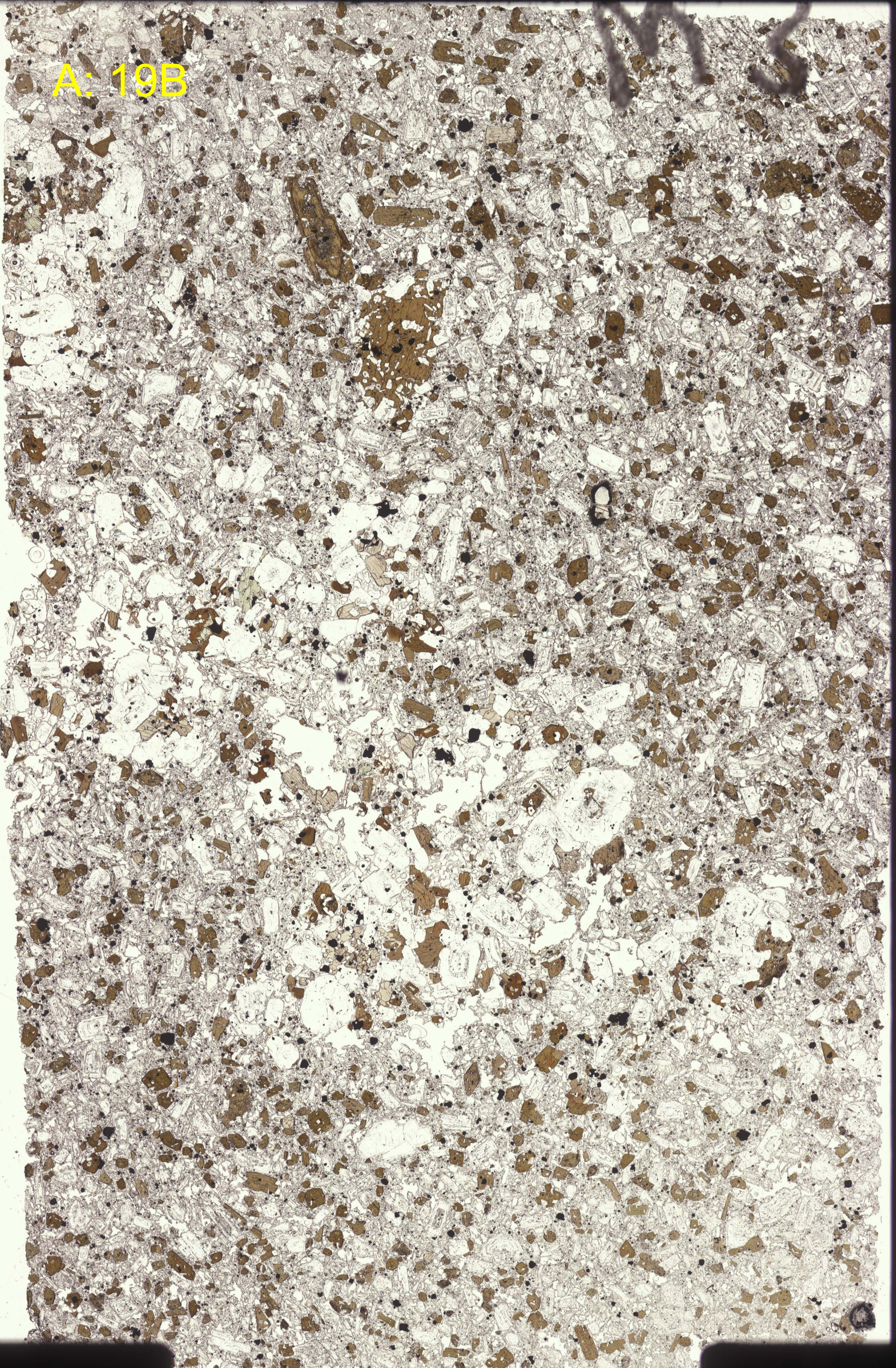
A: 19B

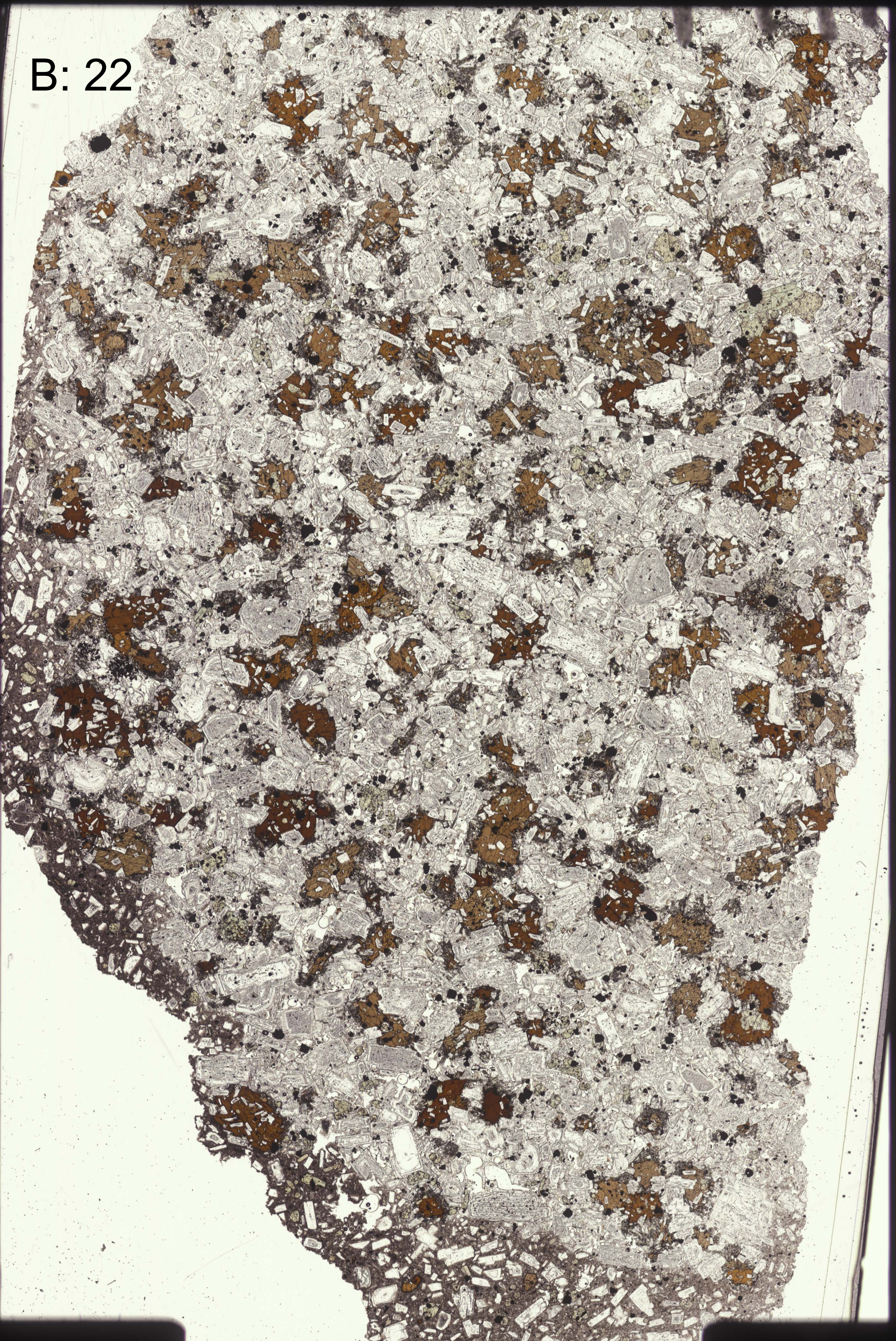
B: 22


C: 24B

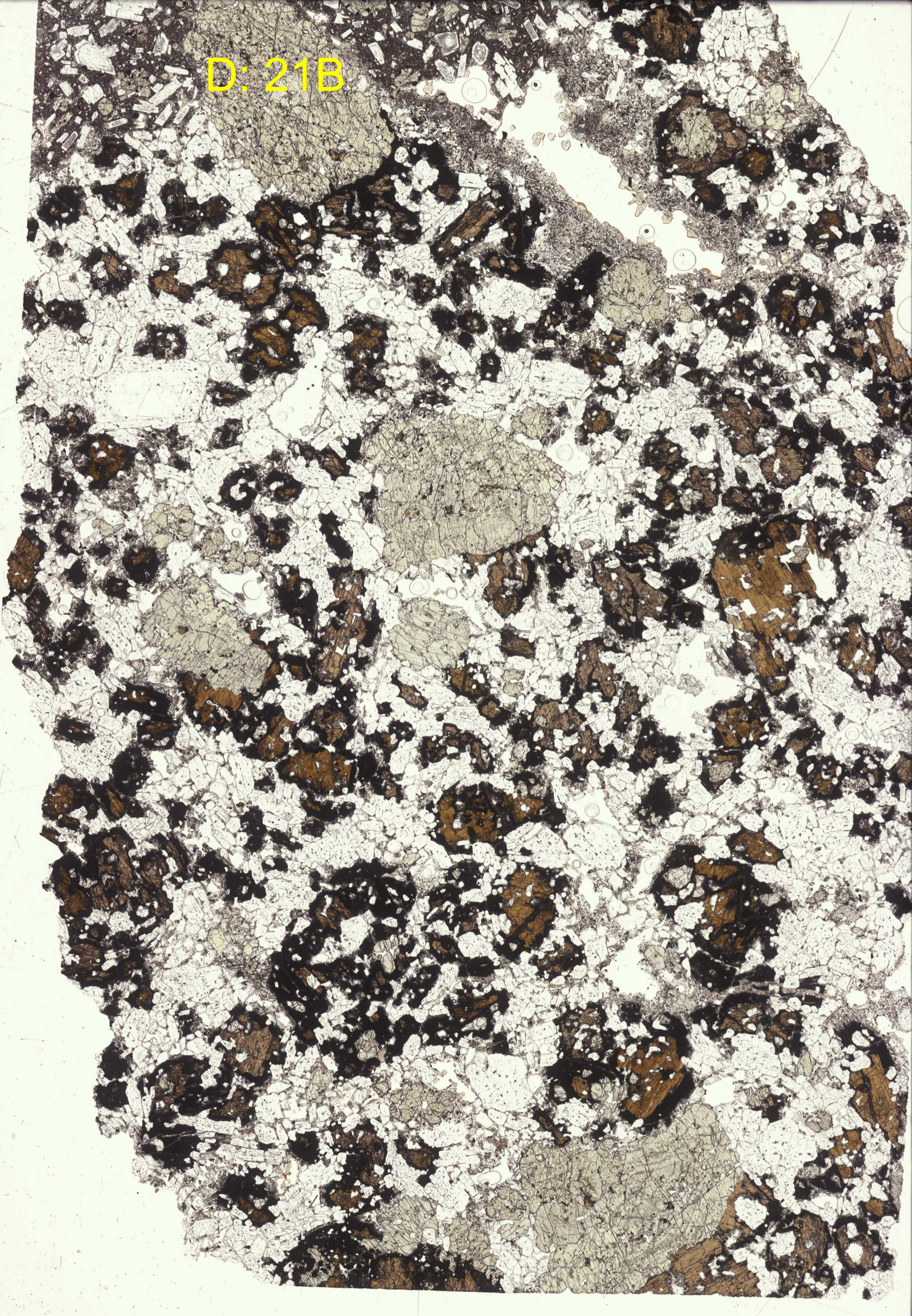
D: 21B

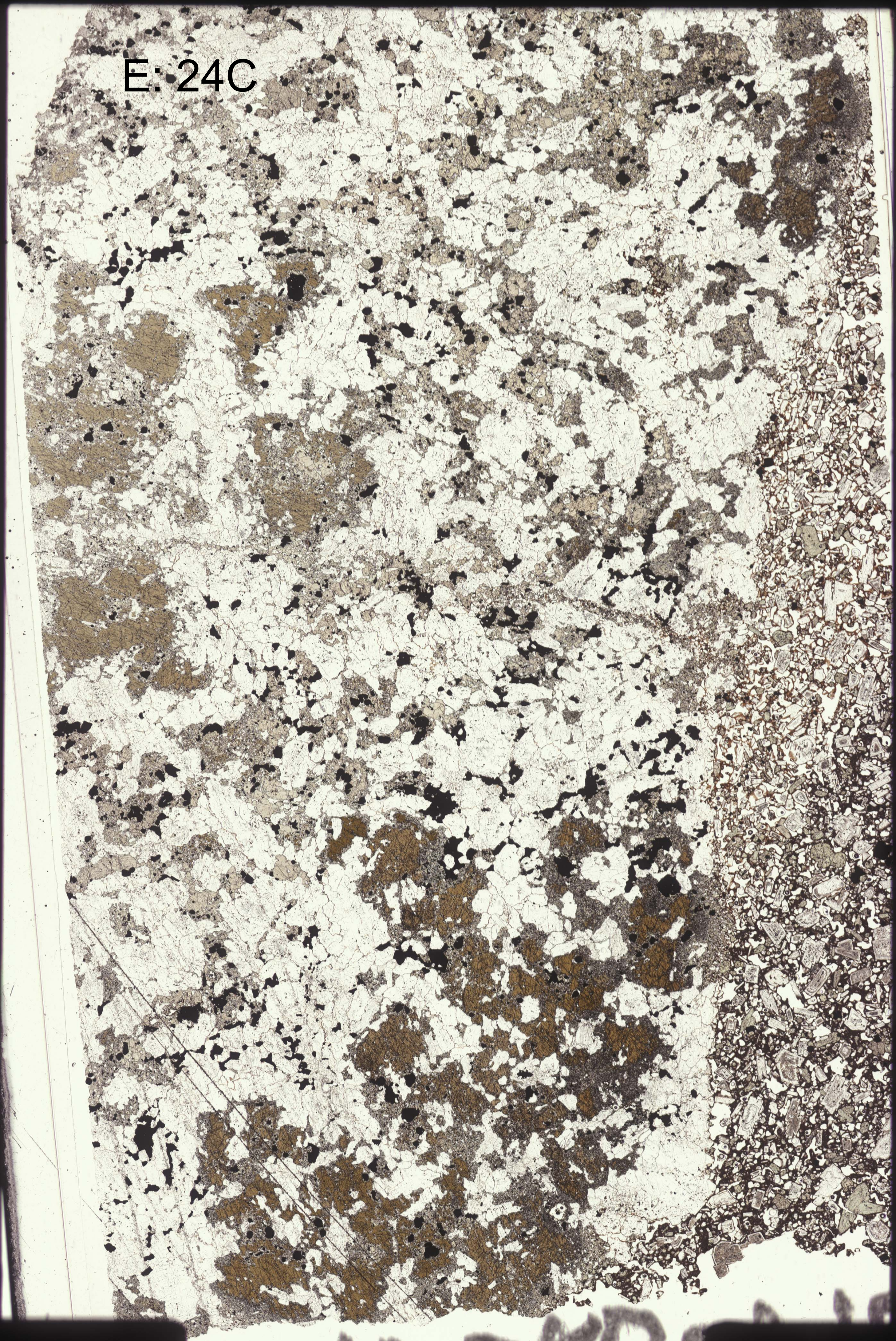
E: 24C

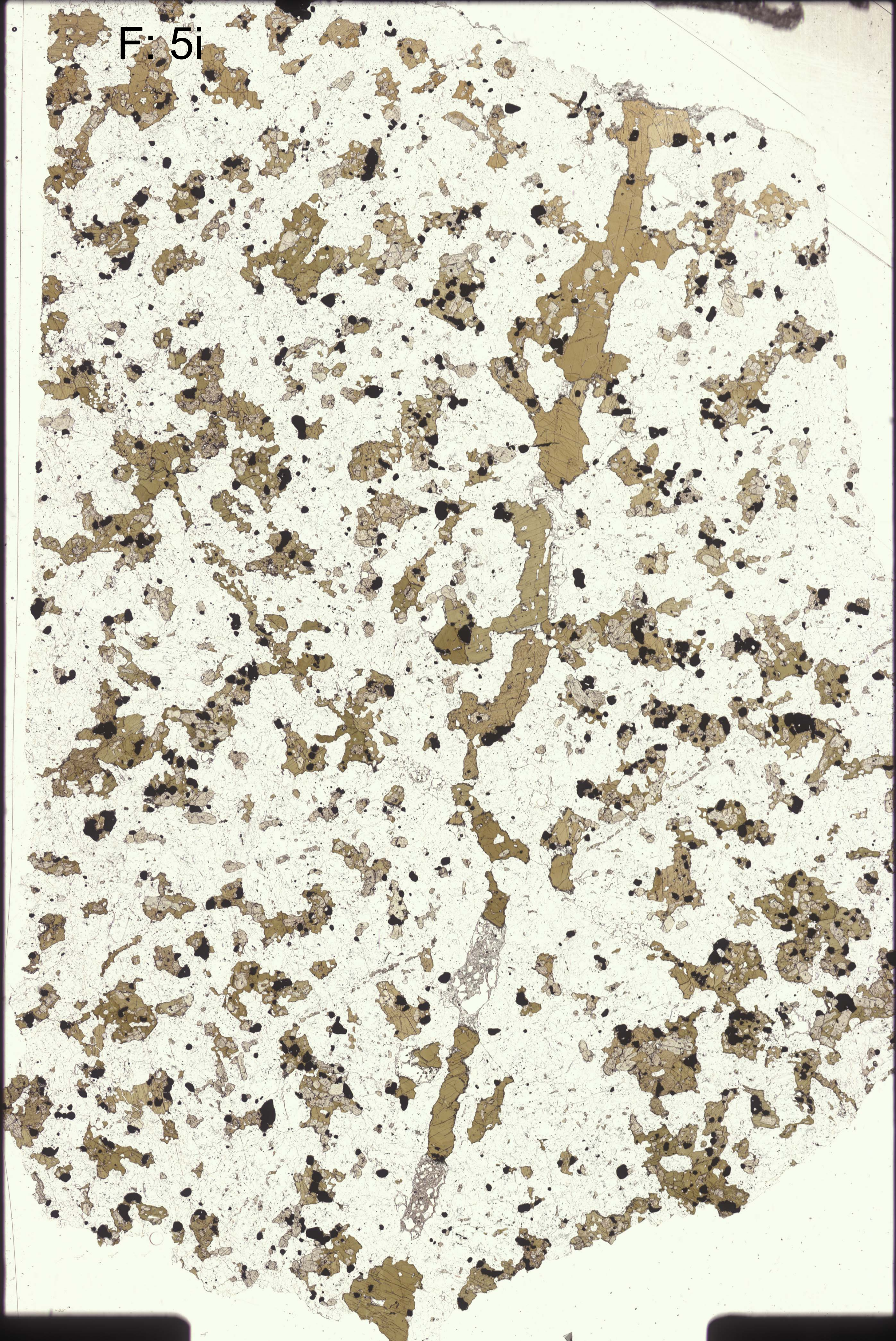
F: 5i

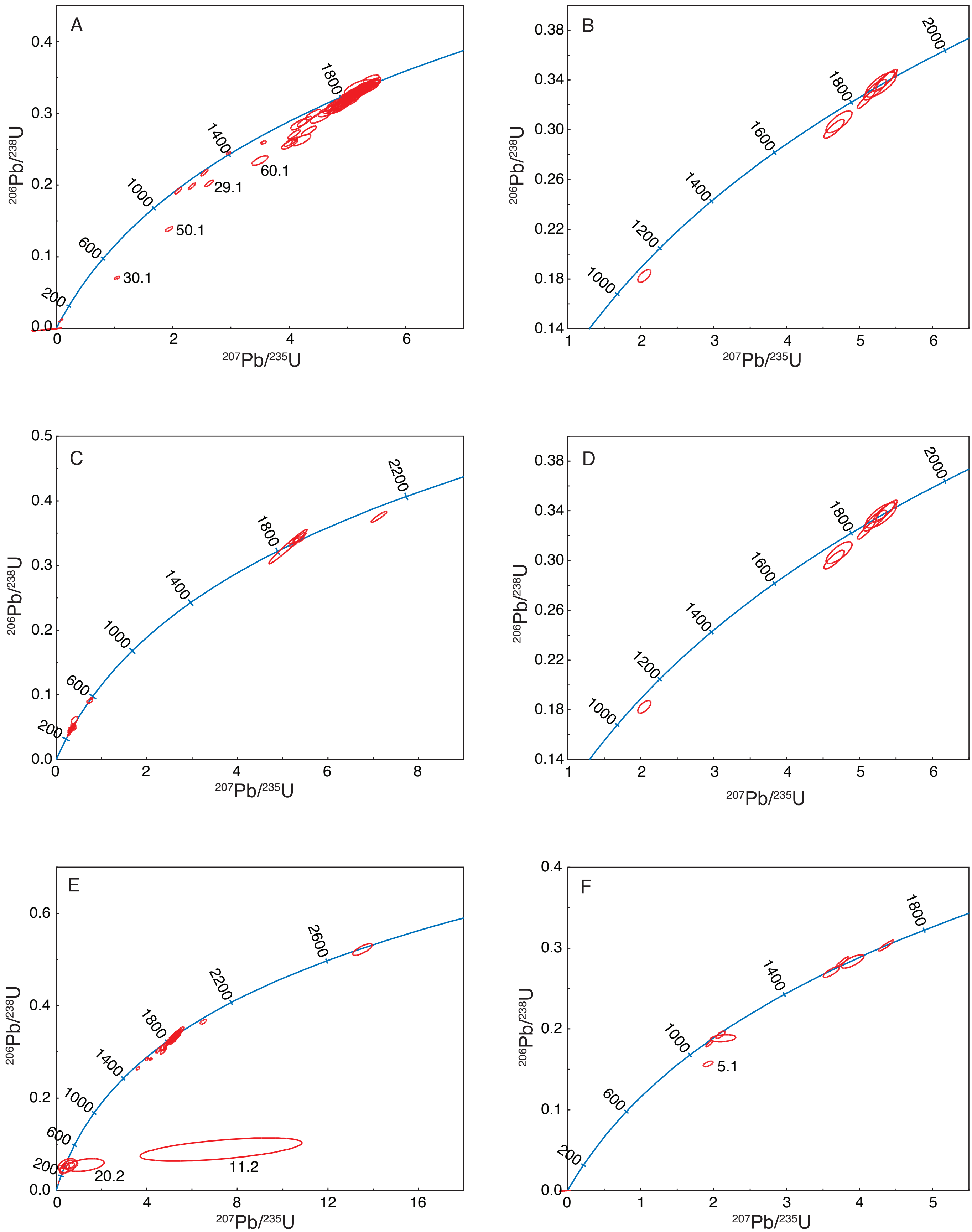

Figure DR2. Concordia diagrams for SHRIMP-RG zircon U–Pb data. Uncertainties for error ellipses are ±2σ. Numbers by blue concordia curves are ages in Ma. Numbers adjacent to select error ellipses identify specific spot analyses. A: Crystal-rich andesite 19B. B: Gabbro 22. C: Gabbro 24B. D: Gabbro 21B. E: Gabbro 24C. F: Gabbro 5i.

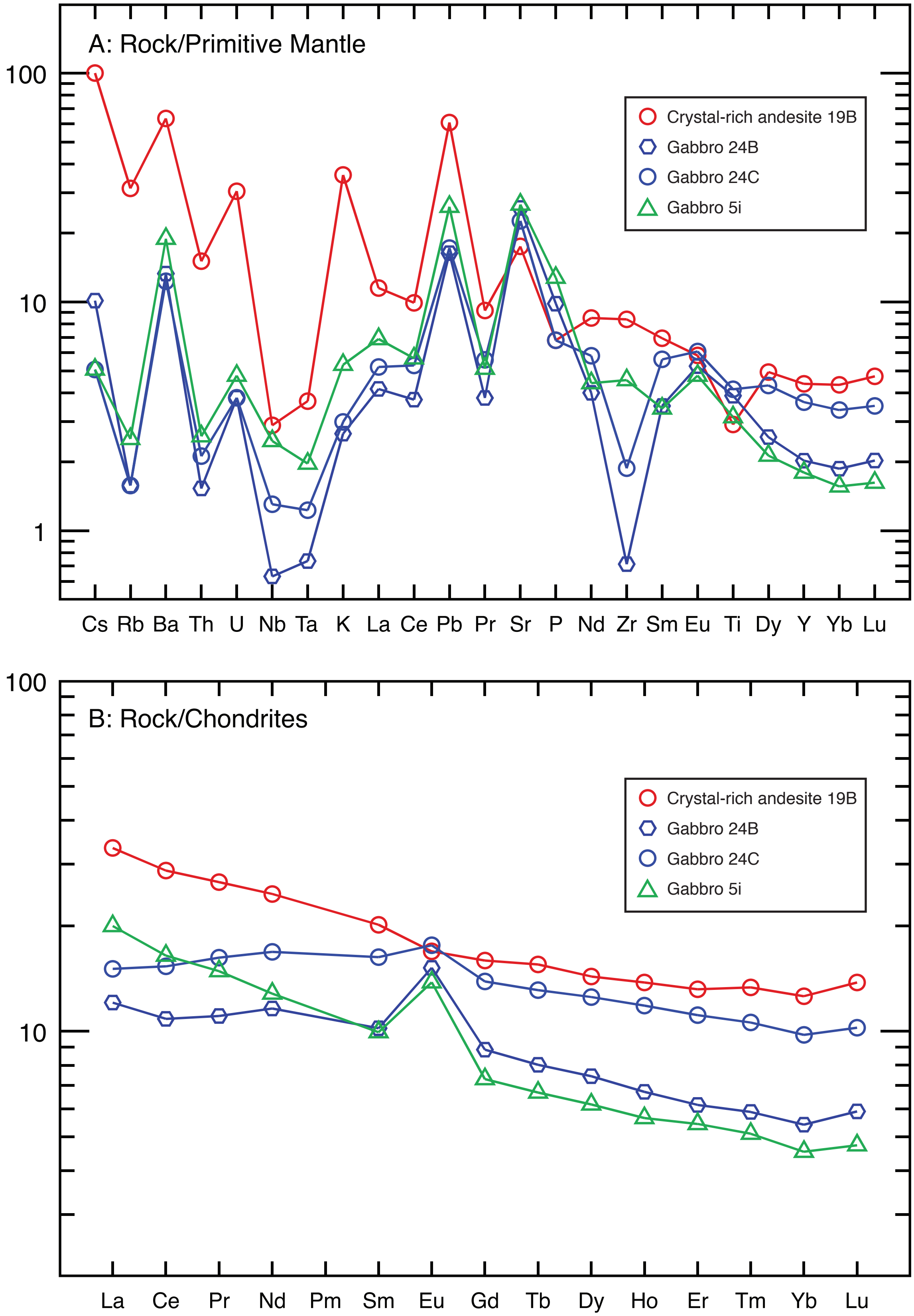

Figure DR3. Whole rock compositions of xenoliths and crystal-rich andesite from Redoubt Volcano.
A: Elemental abundances normalized to primitive mantle values (Sun and McDonough, 1989).
B: Rare earth element abundances normalized to chondrite values (Sun and McDonough, 1989).

Figure DR4. Cathodoluminescence images of zircons from xenoliths from Redoubt Volcano. Images of polished grain mounts were obtained with a JEOL scanning electron microscope. Sample number appears at top of image (e.g., 08RDCRB019B). All CL images are shown, including those for which no zircons were analyzed. Numbers by individual zircons identify analyses, e.g., 72.1 is zircon 72, analysis spot 1 in the sample. Numbers with uncertainties listed, e.g., 1861±8, are $^{238}U/^{206}Pb$ (<1000 Ma) or $^{207}Pb/^{206}Pb$ (≥1000 Ma) ages in Ma; uncertainties are ±1σ (D indicates analysis was >10% discordant). For two grains (08RDCRB019B zircon 62 and 90CNR05i zircon 1), ^{238}U–^{230}Th disequilibrium model ages are given; these are identified by units of ka. Uranium concentrations are given in separate CL images of low-U zircons.

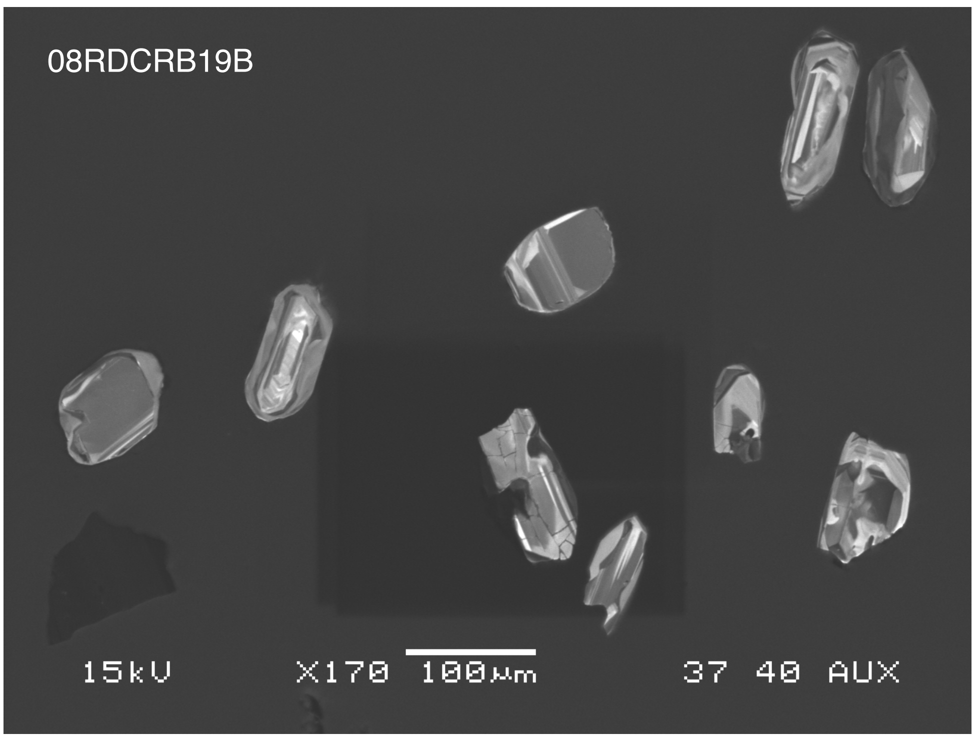
08RDCRB19B
15kV
X170 100µm
37 40 AUX

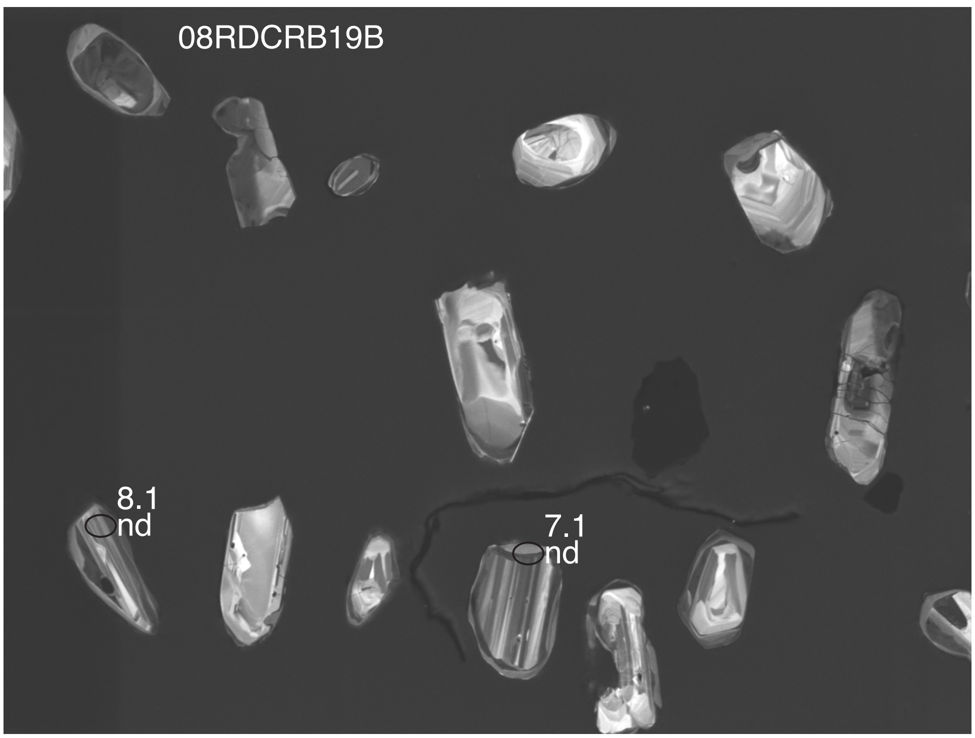
08RDCRB19B
8.1
nd
7.1
nd

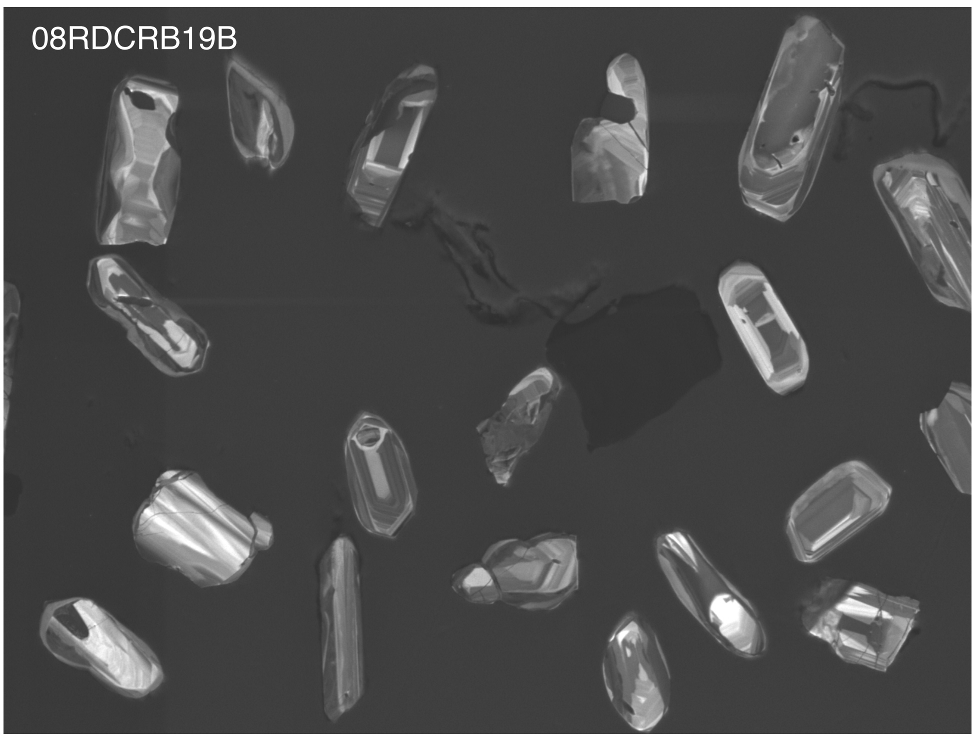
08RDCRB19B

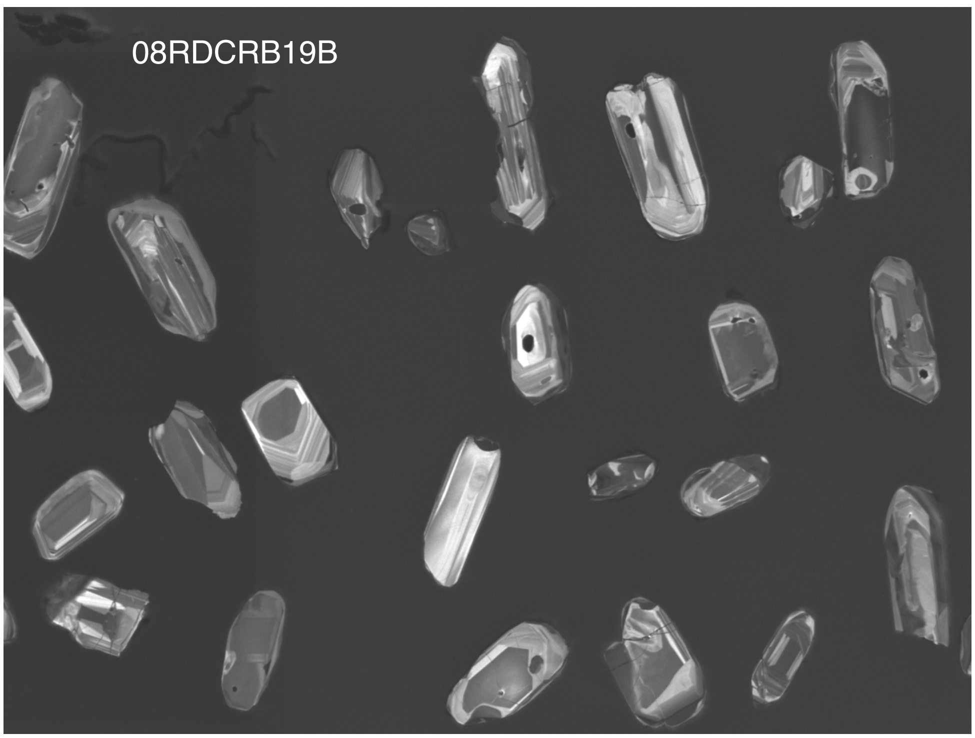
08RDCRB19B

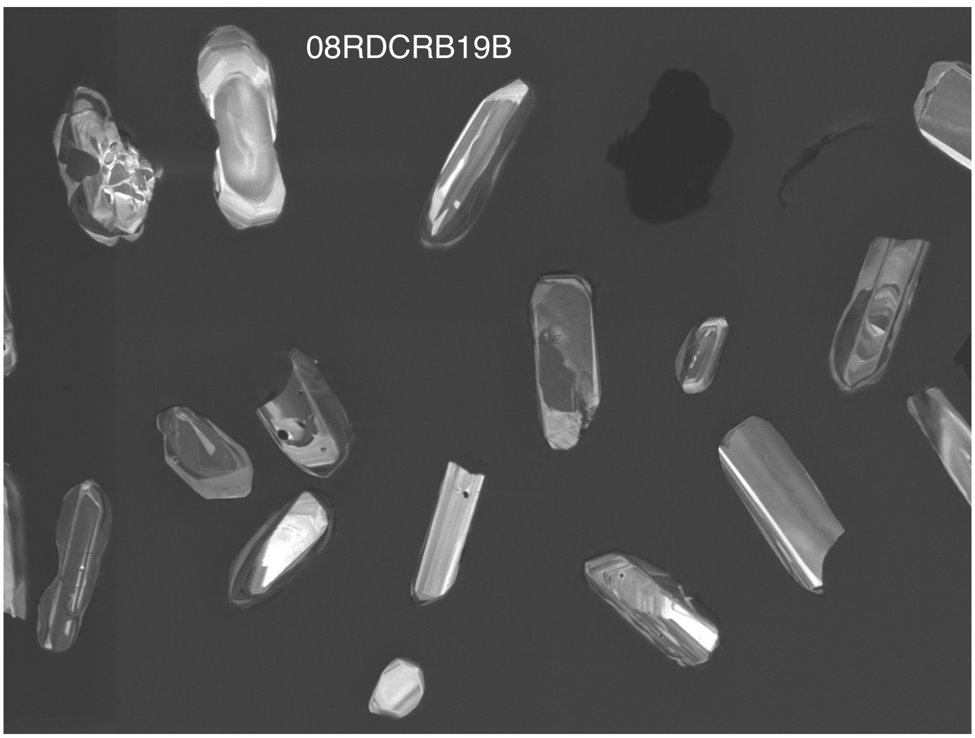
08RDCRB19B

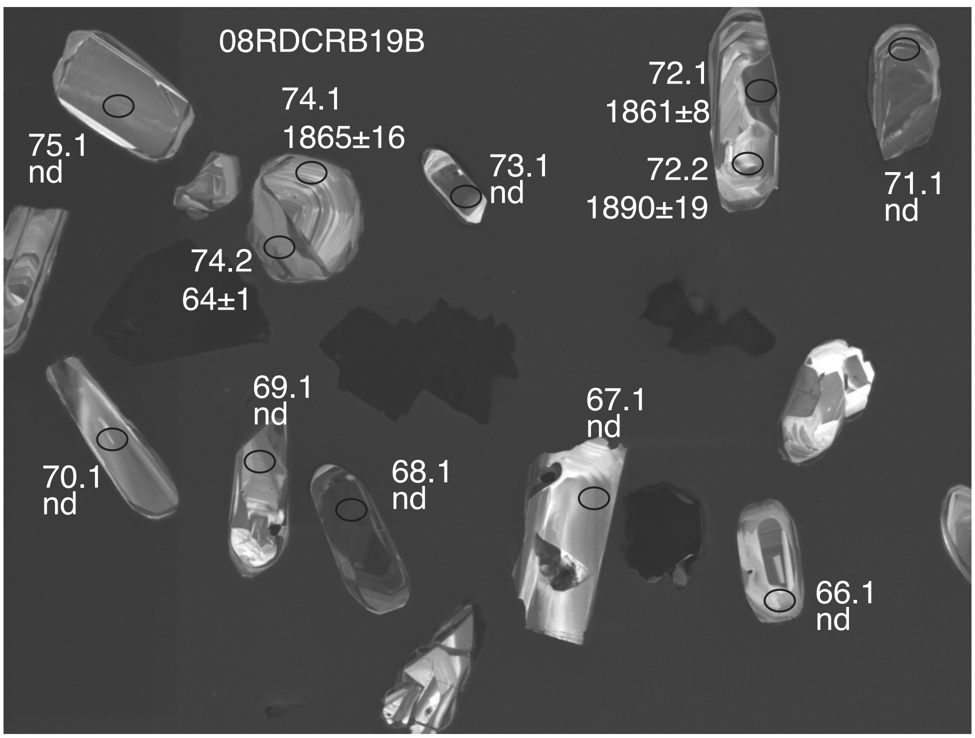
08RDCRB19B
75.1
nd
74.1
1865±16
73.1
nd
72.1
1861±8
72.2
1890±19
71.1
nd
74.2
64±1
69.1
nd
70.1
nd
68.1
nd
67.1
nd
66.1
nd

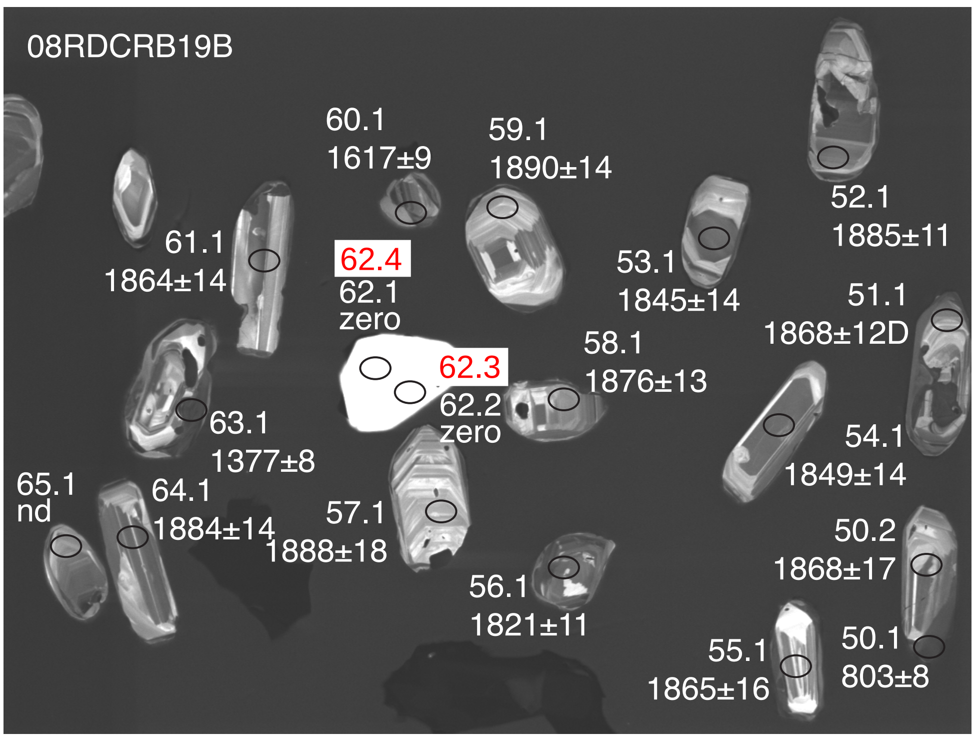

08RDCRB19B
60.1
1617±9
59.1
1890±14
52.1
1885±11
61.1
1864±14
62.4
62.1
zero
53.1
1845±14
51.1
1868±12D
62.3
62.2
zero
58.1
1876±13
63.1
1377±8
54.1
1849±14
65.1
nd
64.1
1884±14
57.1
1888±18
50.2
1868±17
56.1
1821±11
55.1
1865±16
50.1
803±8

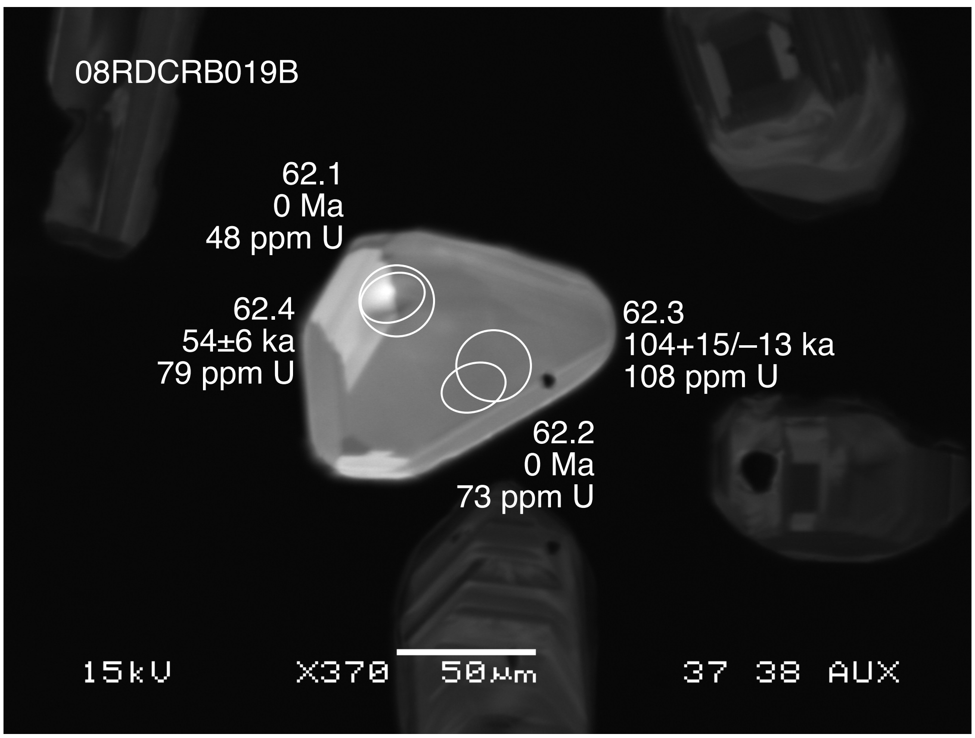
08RDCRB019B
62.1
0 Ma
48 ppm U
62.4
54±6 ka
79 ppm U
62.3
104+15/–13 ka
108 ppm U
62.2
0 Ma
73 ppm U
15kV
X370
50µm
37 38 AUX

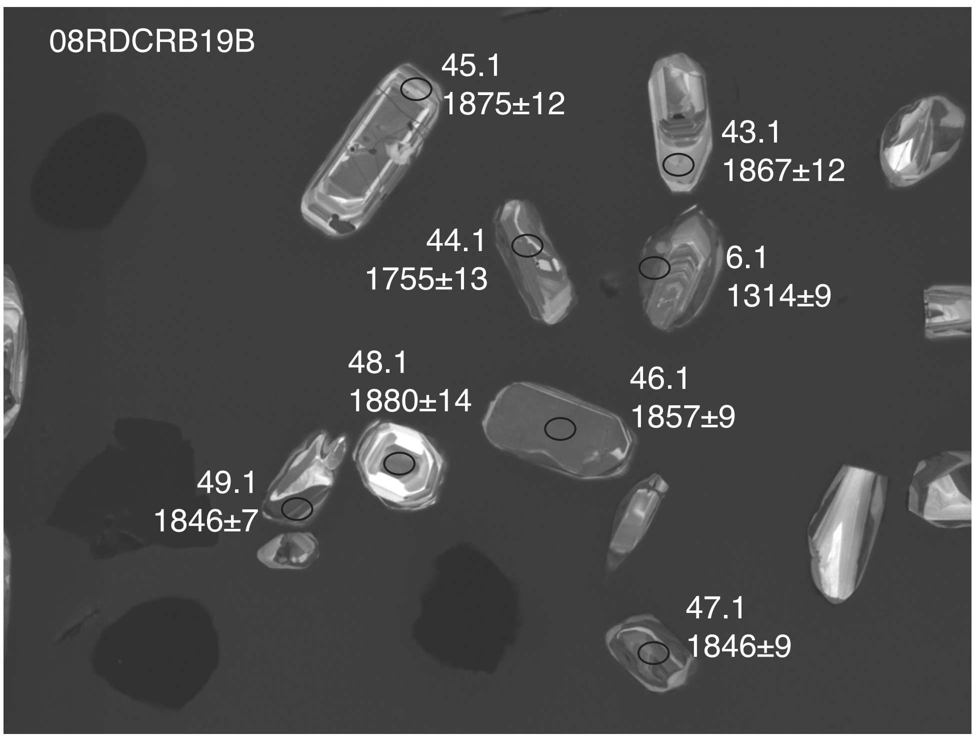
08RDCRB19B
45.1
1875±12
43.1
1867±12
44.1
1755±13
6.1
1314±9
48.1
1880±14
46.1
1857±9
49.1
1846±7
47.1
1846±9

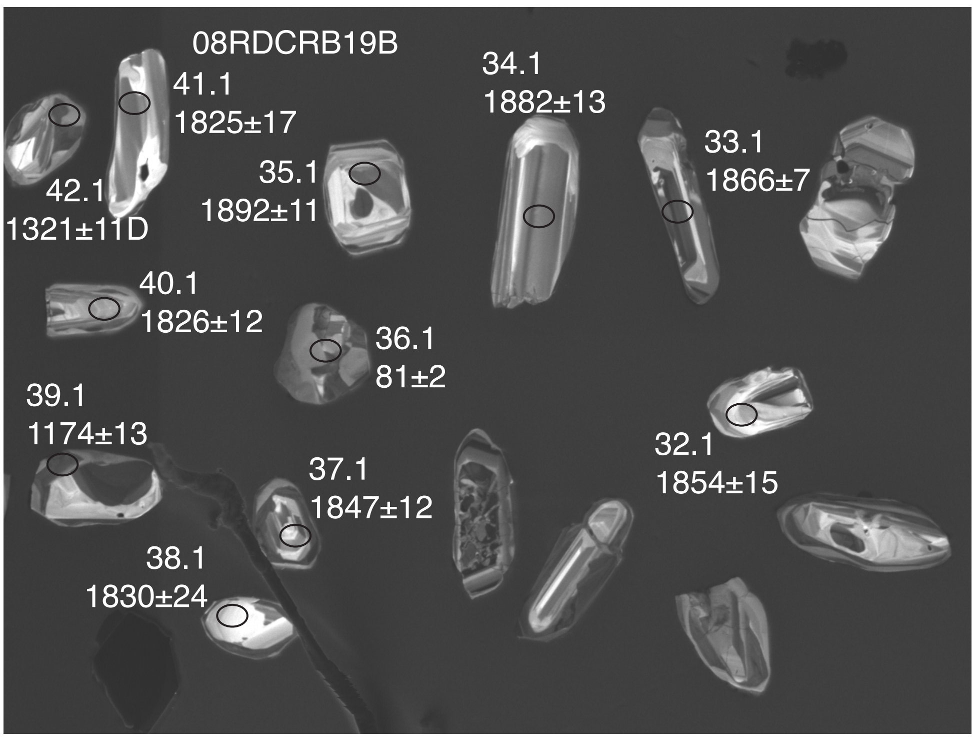
08RDCRB19B
41.1
1825±17
34.1
1882±13
33.1
1866±7
35.1
1892±11
42.1
1321±11D
40.1
1826±12
36.1
81±2
39.1
1174±13
32.1
1854±15
37.1
1847±12
38.1
1830±24

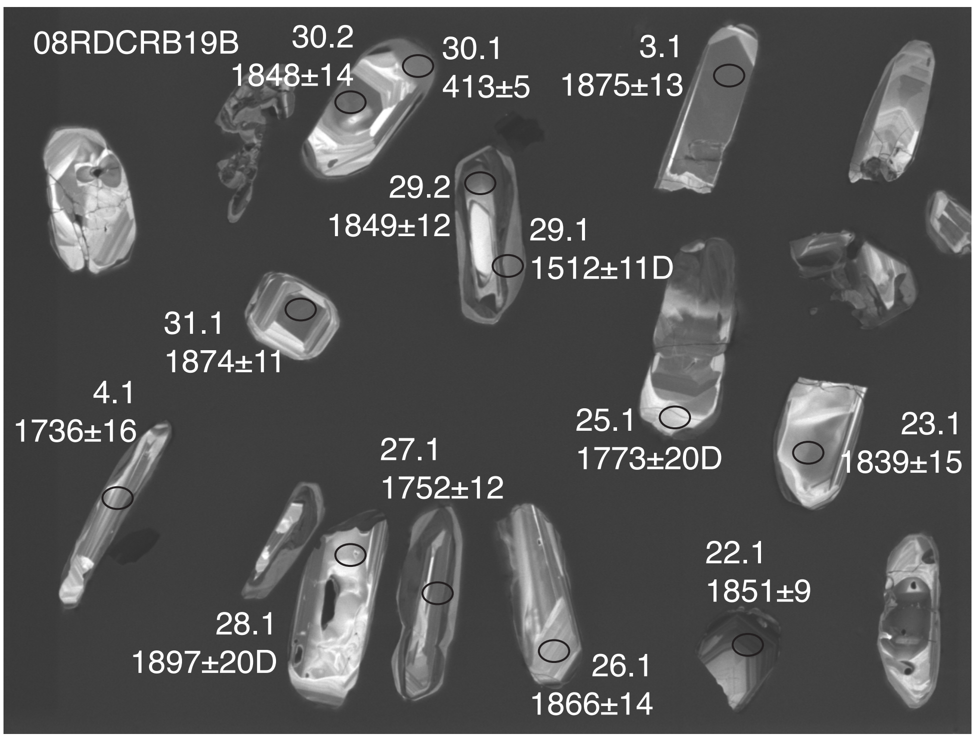

08RDCRB19B
30.2
1848±14
30.1
413±5
3.1
1875±13
29.2
1849±12
29.1
1512±11D
31.1
1874±11
4.1
1736±16
25.1
1773±20D
23.1
1839±15
27.1
1752±12
22.1
1851±9
28.1
1897±20D
26.1
1866±14

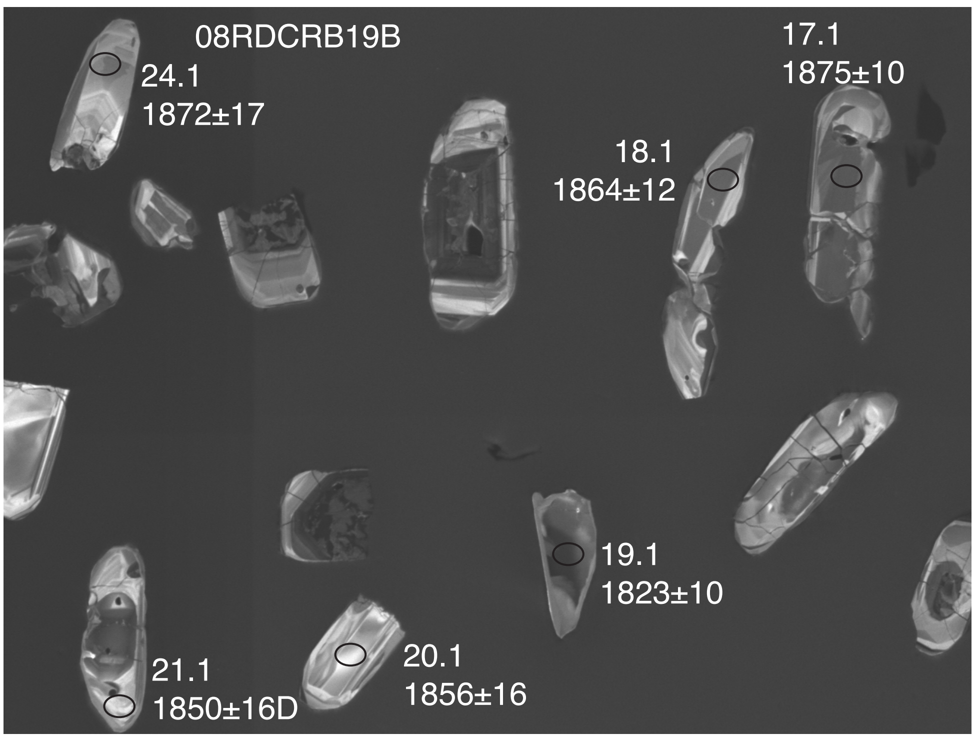
08RDCRB19B
24.1
1872±17
17.1
1875±10
18.1
1864±12
19.1
1823±10
21.1
1850±16D
20.1
1856±16

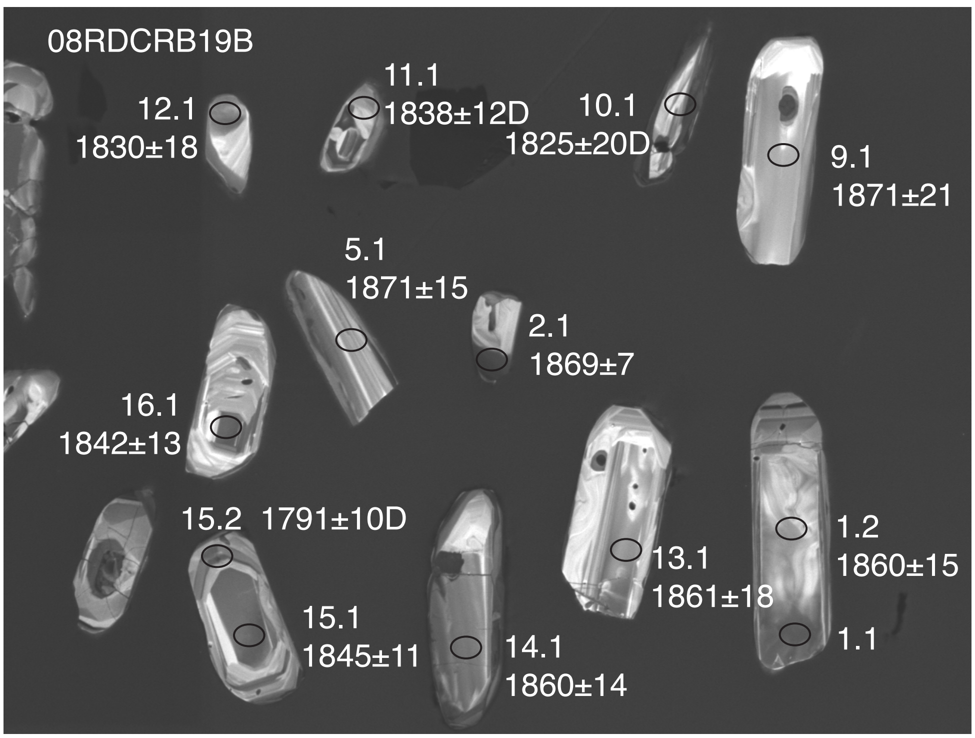
08RDCRB19B
12.1
1830±18
11.1
1838±12D
10.1
1825±20D
9.1
1871±21
5.1
1871±15
2.1
1869±7
16.1
1842±13
15.2
1791±10D
15.1
1845±11
14.1
1860±14
13.1
1861±18
1.2
1860±15
1.1


08RDCRB22
8.1
1233±26D

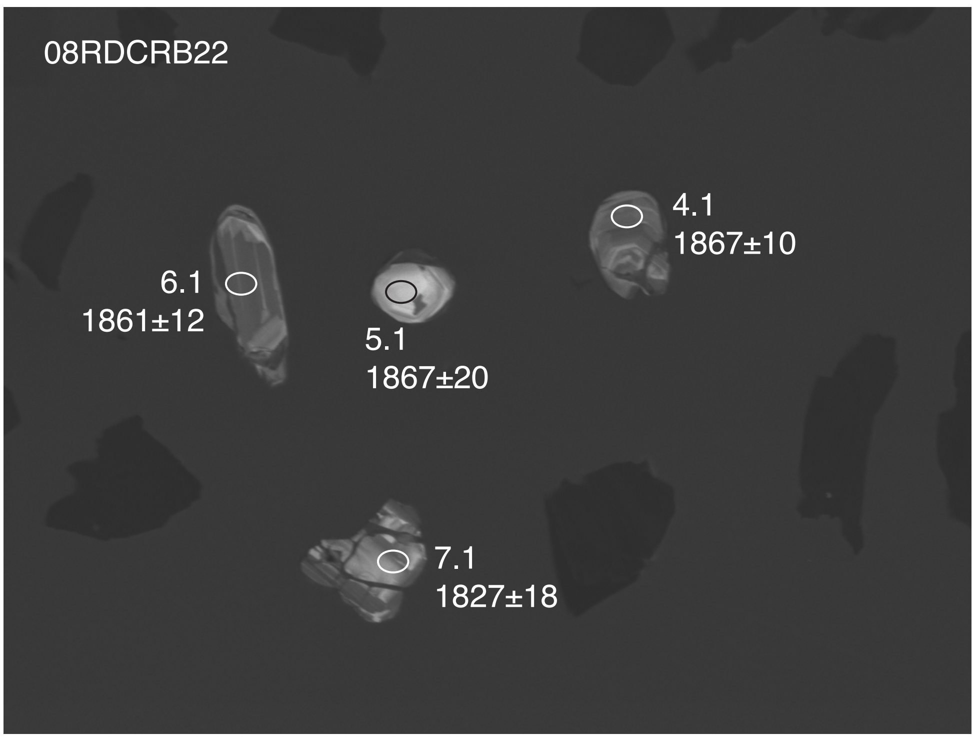
08RDCRB22
4.1
1867±10
6.1
1861±12
5.1
1867±20
7.1
1827±18

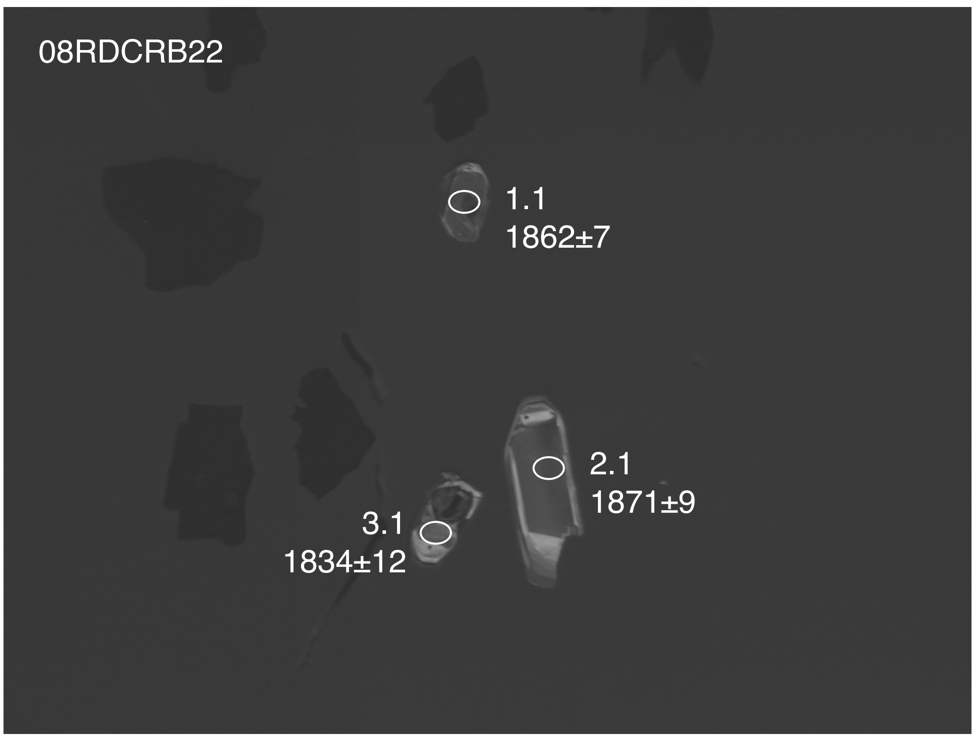
08RDCRB22
1.1
1862±7
2.1
1871±9
3.1
1834±12

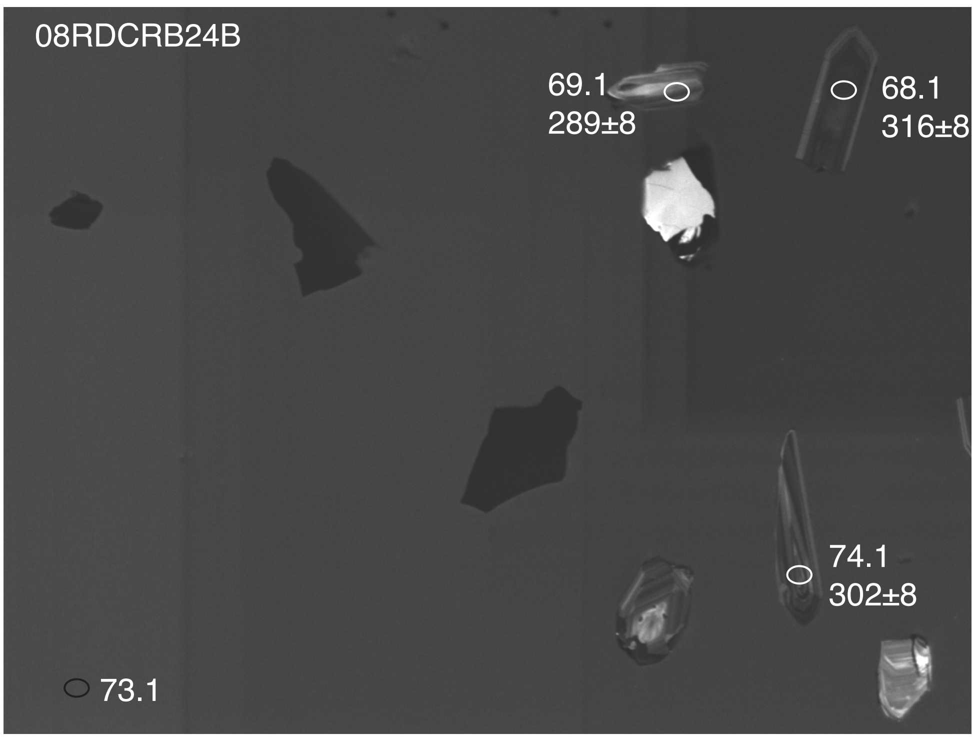
08RDCRB24B
69.1
289±8
68.1
316±8
74.1
302±8
73.1

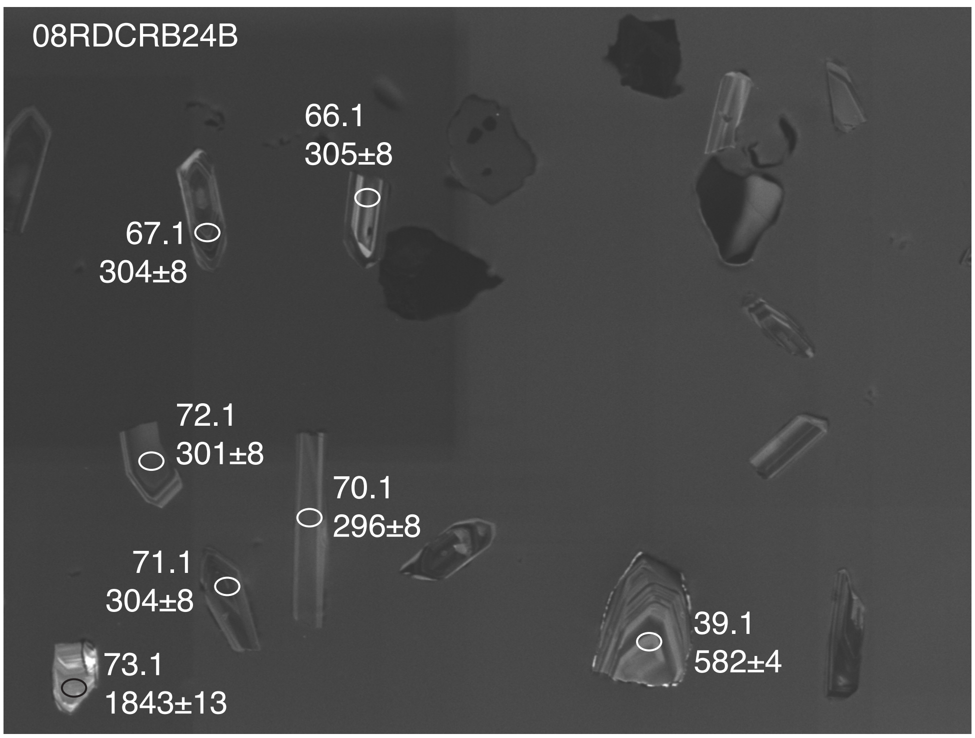
08RDCRB24B
66.1
305±8
67.1
304±8
72.1
301±8
70.1
296±8
71.1
304±8
73.1
1843±13
39.1
582±4


08RDCRB24B
46.1
283±8
47.1
286±8
48.1
282±8
49.1
300±8
53.1
304±8
50.1
291±8
52.1
304±8
51.1
299±8
41.1
282±8
43.1
286±8
44.1
296±8
45.1
307±8
38.1
nd
42.1
294±8
37.1
312±2

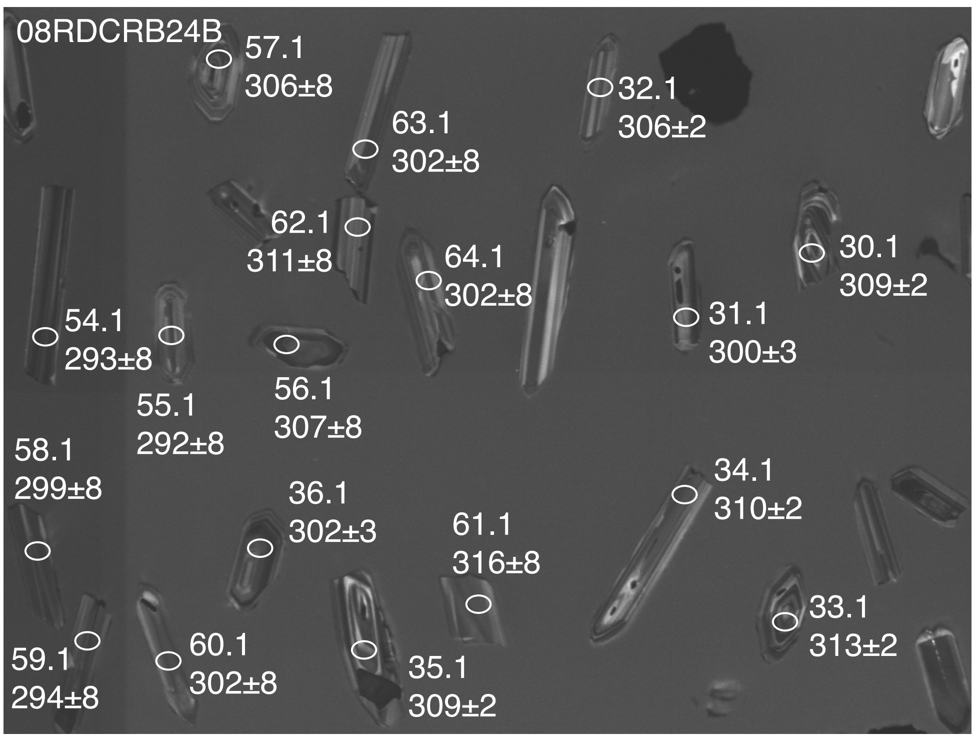
08RDCRB24B
57.1
306±8
63.1
302±8
32.1
306±2
62.1
311±8
64.1
302±8
30.1
309±2
31.1
300±3
54.1
293±8
55.1
292±8
56.1
307±8
58.1
299±8
36.1
302±3
61.1
316±8
34.1
310±2
33.1
313±2
59.1
294±8
60.1
302±8
35.1
309±2

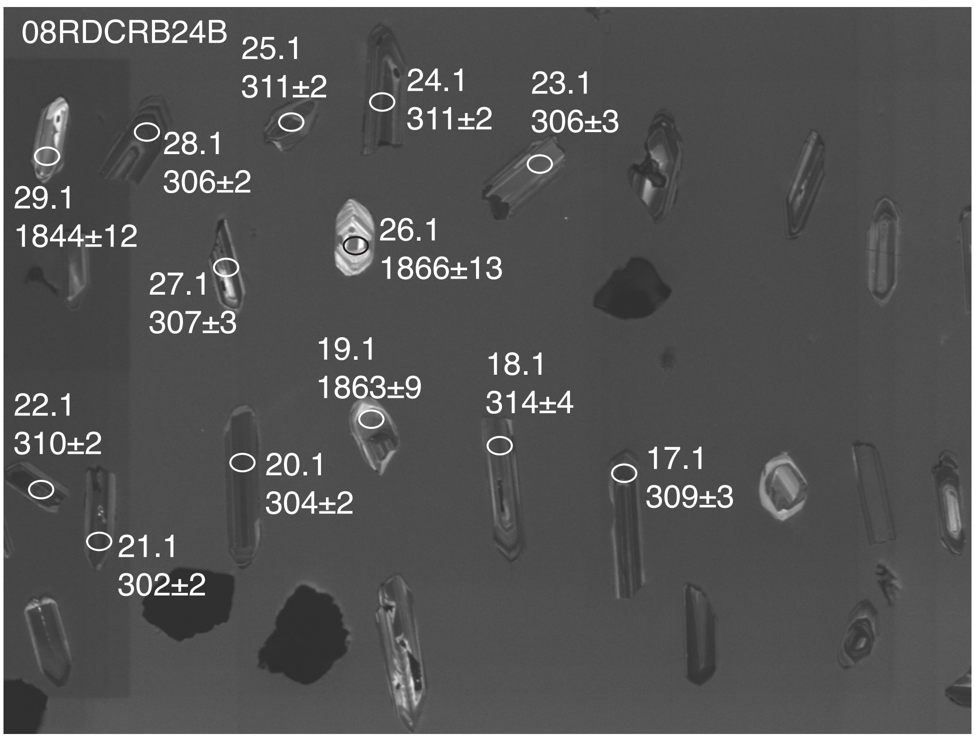

08RDCRB24B
25.1
311±2
24.1
311±2
23.1
306±3
28.1
306±2
29.1
1844±12
26.1
1866±13
27.1
307±3
19.1
1863±9
18.1
314±4
22.1
310±2
20.1
304±2
17.1
309±3
21.1
302±2

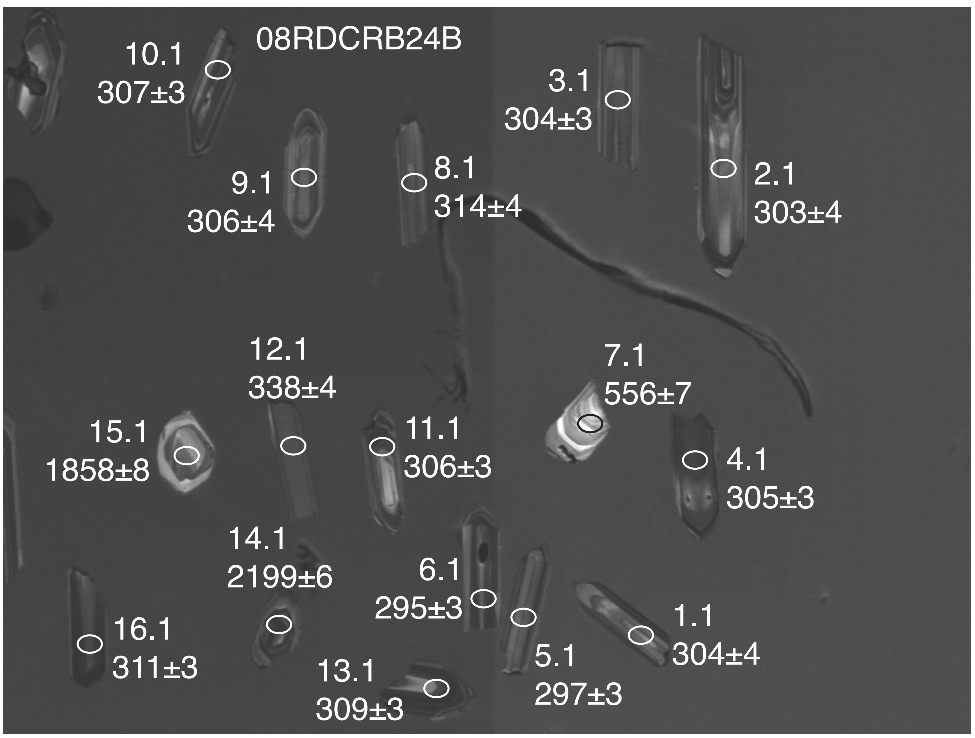
08RDCRB24B
10.1
307±3
3.1
304±3
9.1
306±4
8.1
314±4
2.1
303±4
12.1
338±4
7.1
556±7
15.1
1858±8
11.1
306±3
4.1
305±3
14.1
2199±6
6.1
295±3
1.1
304±4
16.1
311±3
5.1
297±3
13.1
309±3

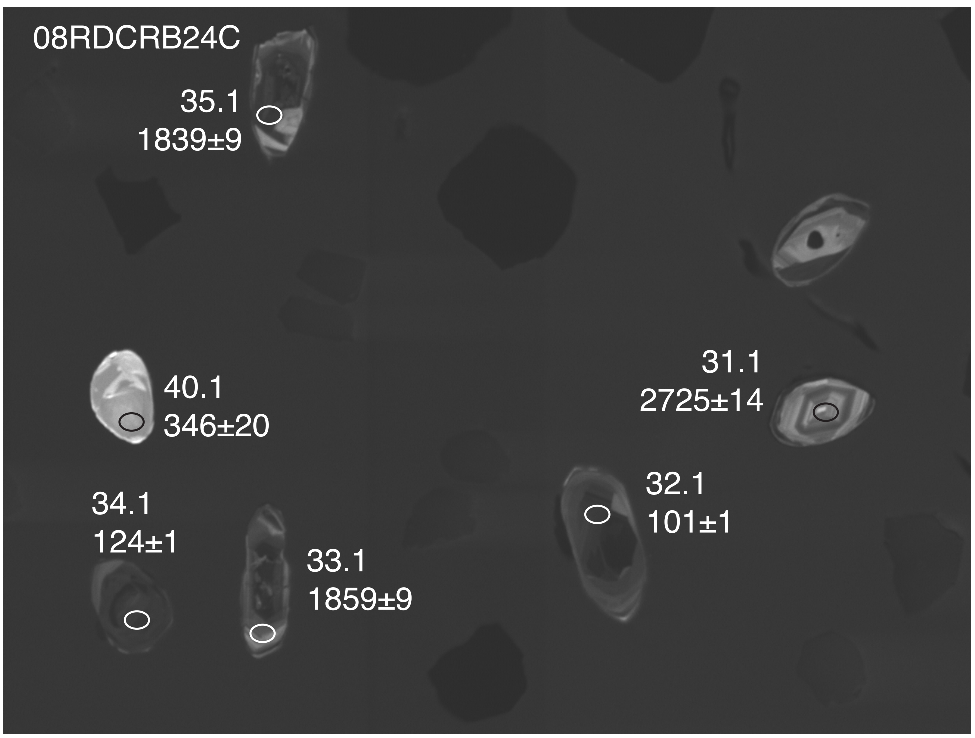
08RDCRB24C
35.1
1839±9
40.1
346±20
31.1
2725±14
32.1
101±1
34.1
124±1
33.1
1859±9

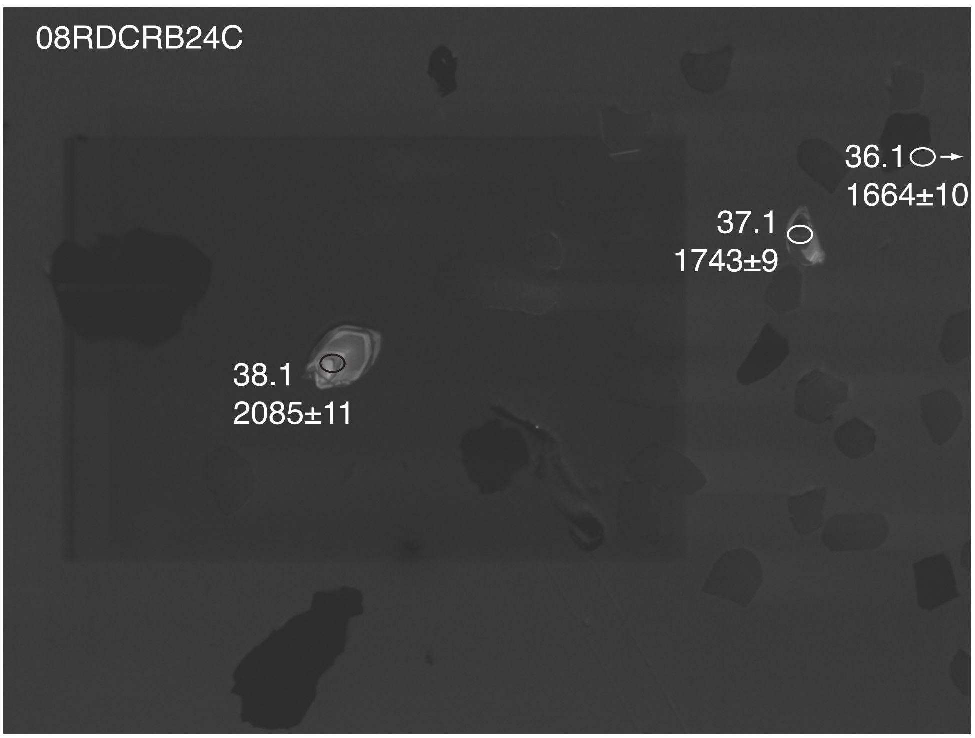
08RDCRB24C
36.1
1664±10
37.1
1743±9
38.1
2085±11

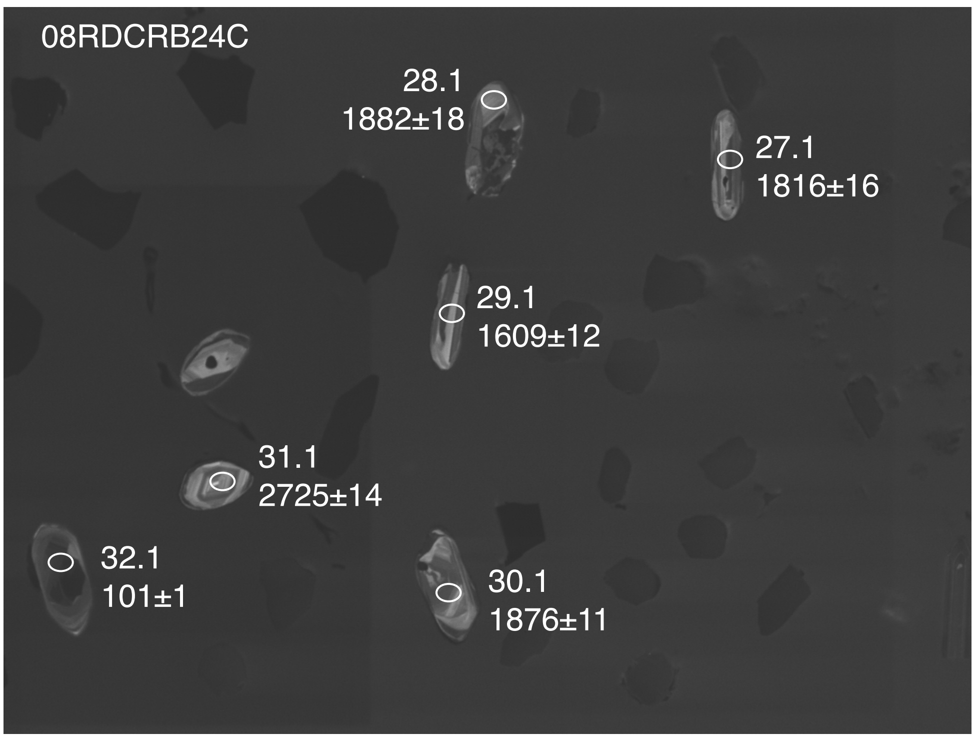

08RDCRB24C
28.1
1882±18
27.1
1816±16
29.1
1609±12
31.1
2725±14
32.1
101±1
30.1
1876±11

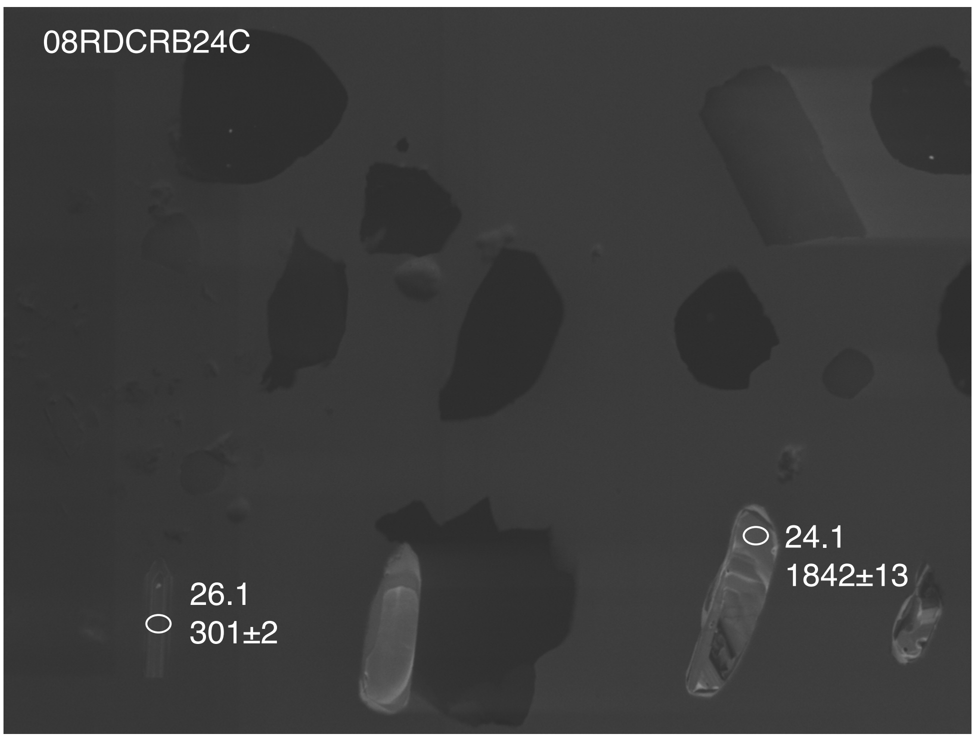
08RDCRB24C
26.1
301±2
24.1
1842±13

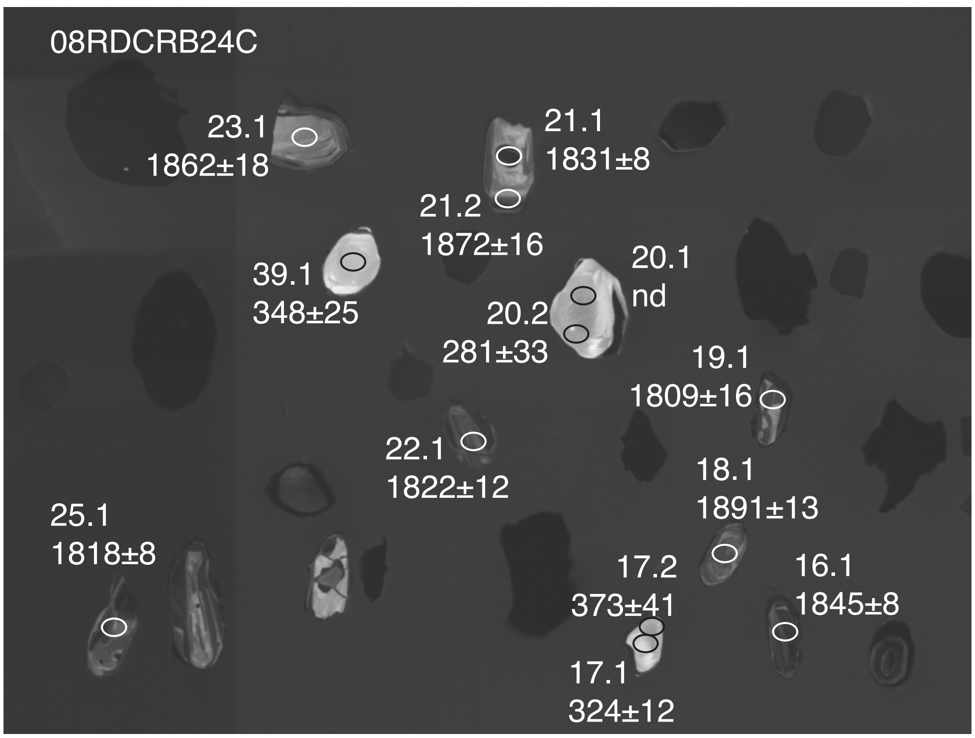
08RDCRB24C
23.1
1862±18
21.1
1831±8
21.2
1872±16
39.1
348±25
20.1
nd
20.2
281±33
19.1
1809±16
22.1
1822±12
18.1
1891±13
25.1
1818±8
17.2
373±41
16.1
1845±8
17.1
324±12

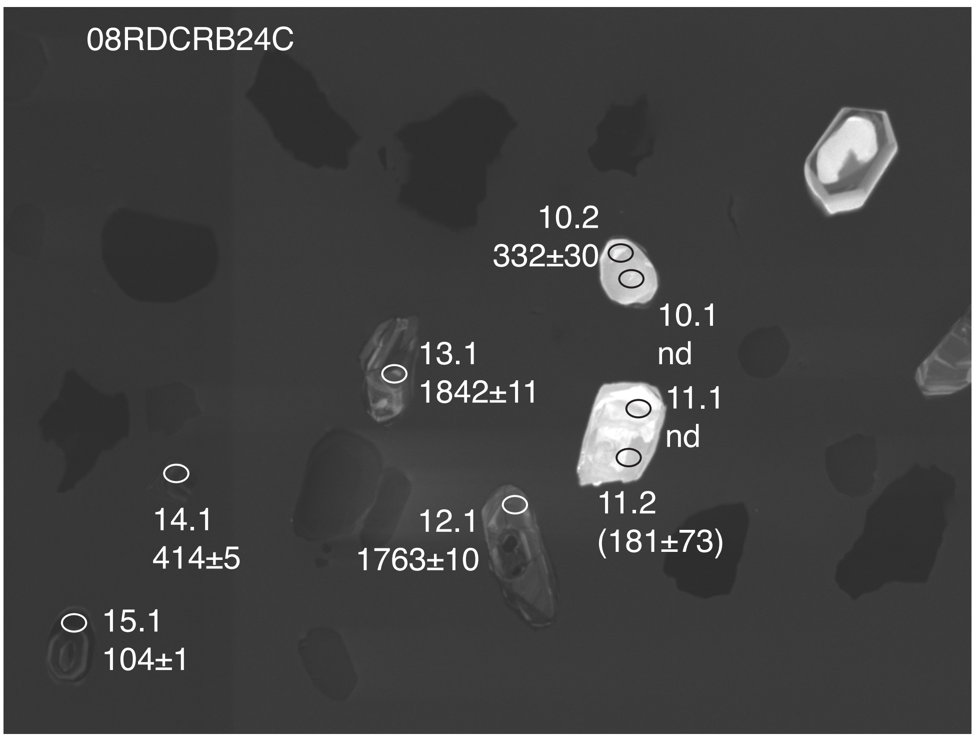

08RDCRB24C
10.2
332±30
10.1
nd
13.1
1842±11
11.1
nd
14.1
414±5
12.1
1763±10
11.2
(181±73)
15.1
104±1

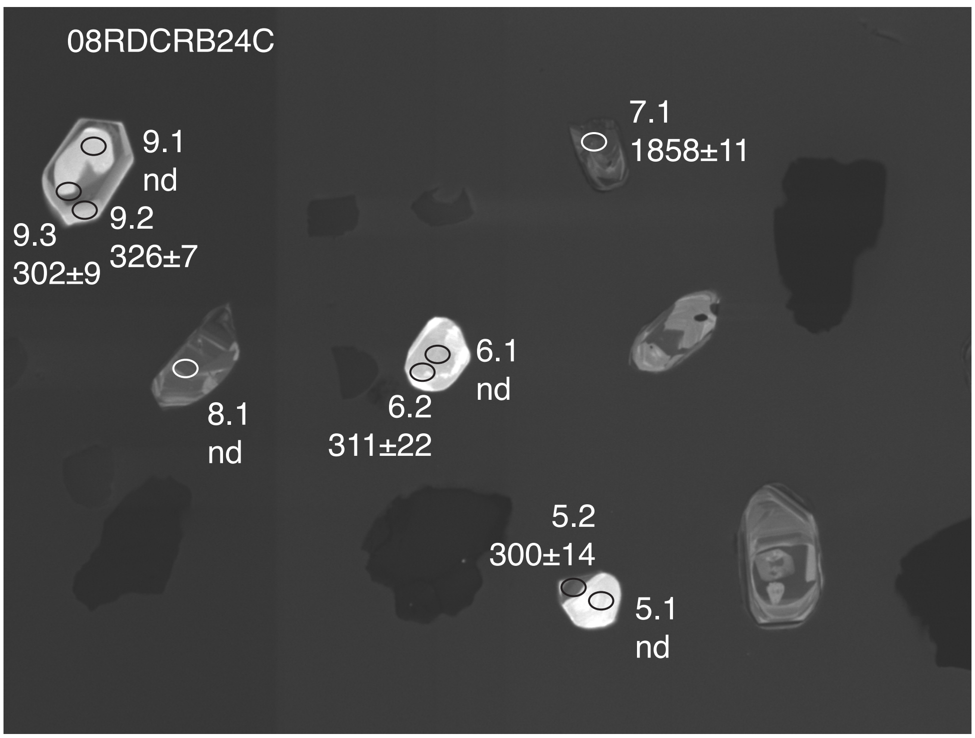
08RDCRB24C
9.1
nd
9.3
302±9
9.2
326±7
7.1
1858±11
8.1
nd
6.1
nd
6.2
311±22
5.2
300±14
5.1
nd


08RDCRB24C
1.1
1880±12
2.1
1868±8
4.1
1856±16
3.1
1870±23

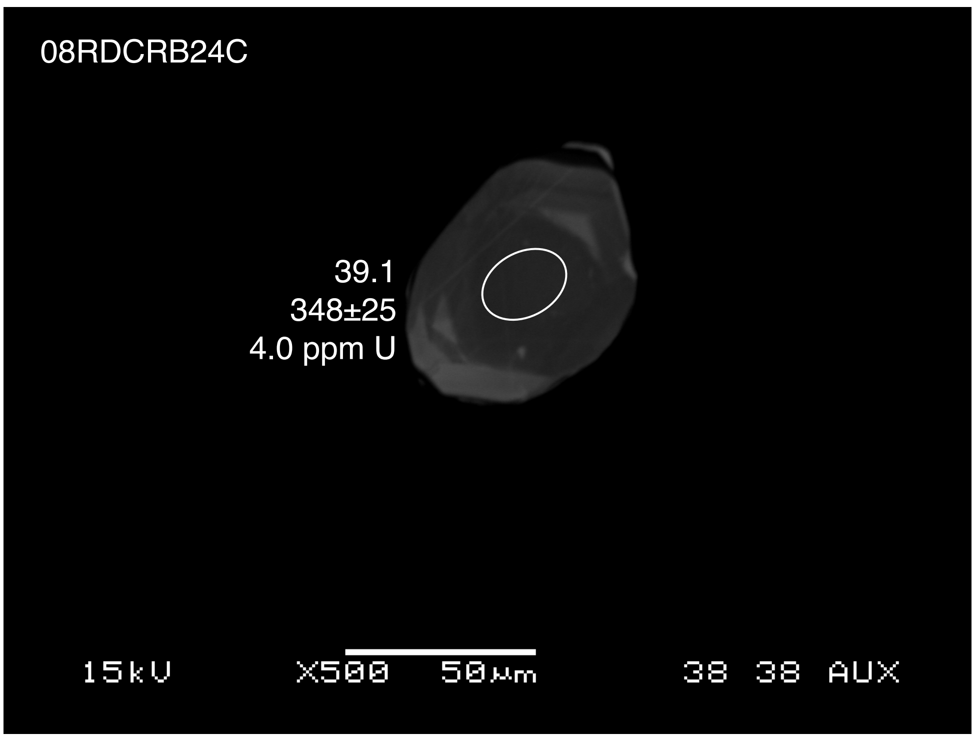
08RDCRB24C
39.1
348±25
4.0 ppm U
15kV
X500
50µm
38 38 AUX


08RDCRB24C
17.2
324±12
22 ppm U
17.1
(373±41)
0.9 ppm U
15kV
X500
50µm
38 38 AUX

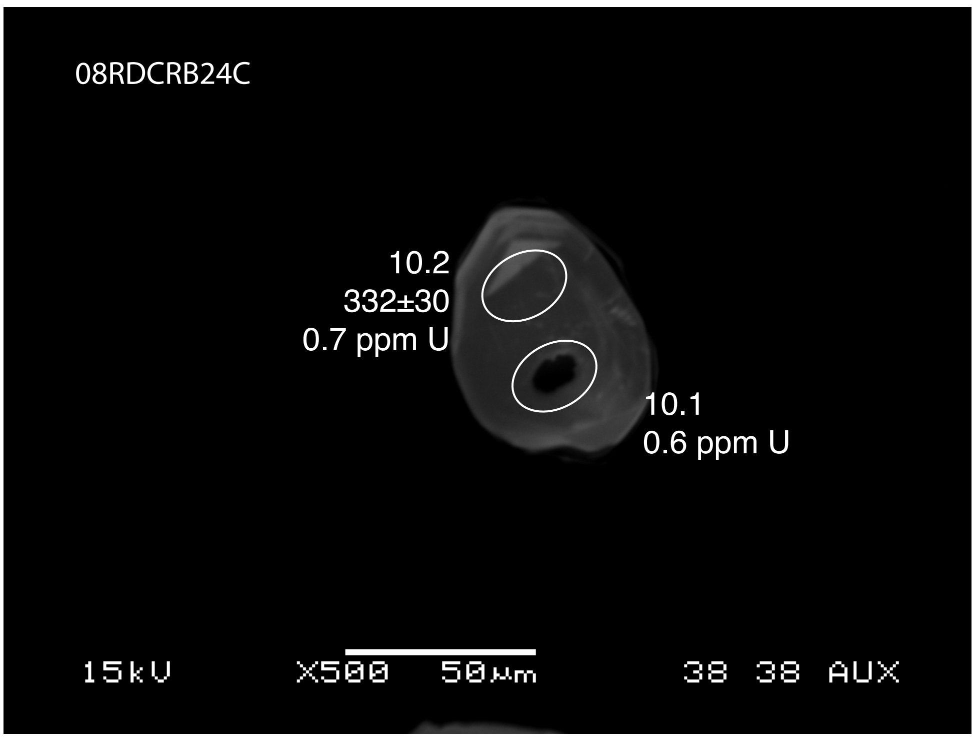

08RDCRB24C
10.2
332±30
0.7 ppm U
10.1
0.6 ppm U
15kV
X500 50µm
38 38 AUX

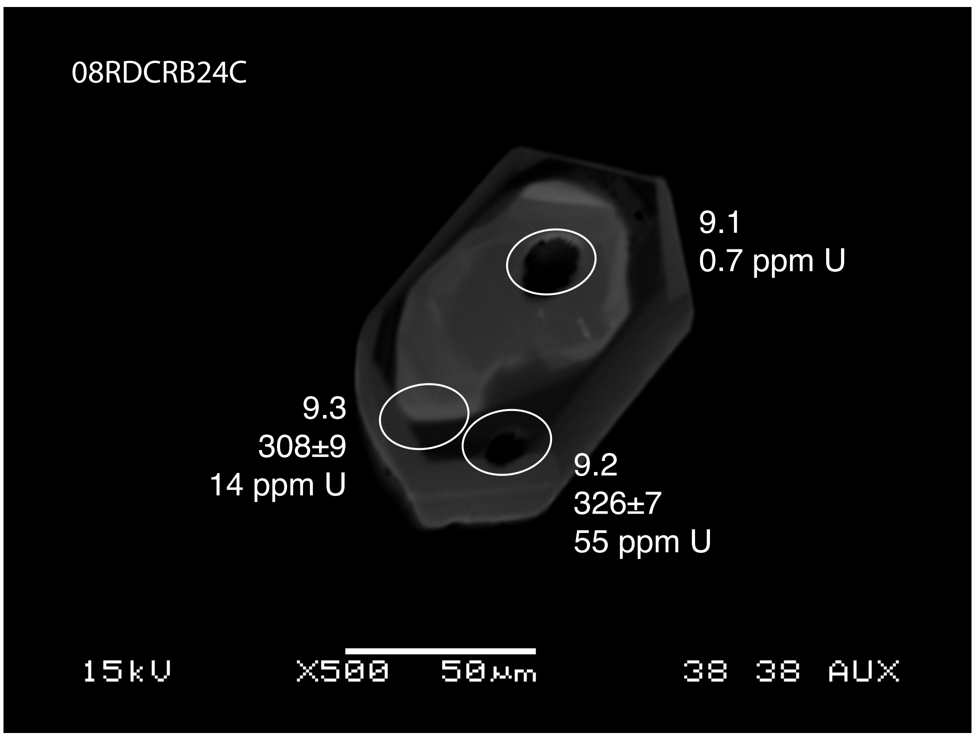
08RDCRB24C
9.1
0.7 ppm U
9.3
308±9
14 ppm U
9.2
326±7
55 ppm U
15kV
X500 50µm
38 38 AUX

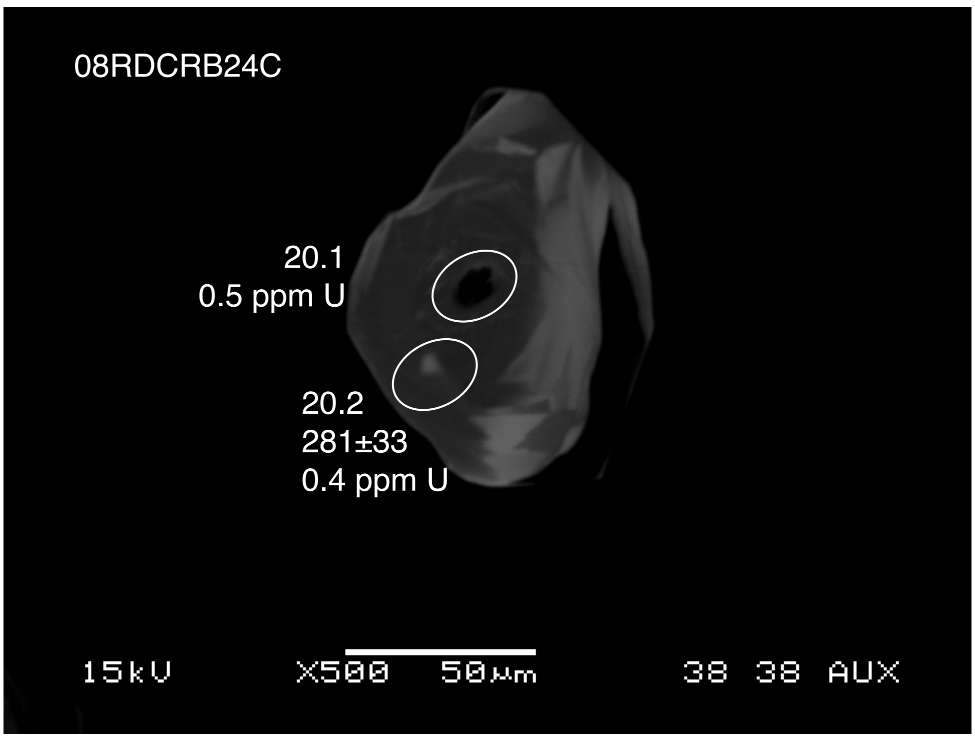
08RDCRB24C
20.1
0.5 ppm U
20.2
281±33
0.4 ppm U
15kV
X500
50µm
38 38 AUX

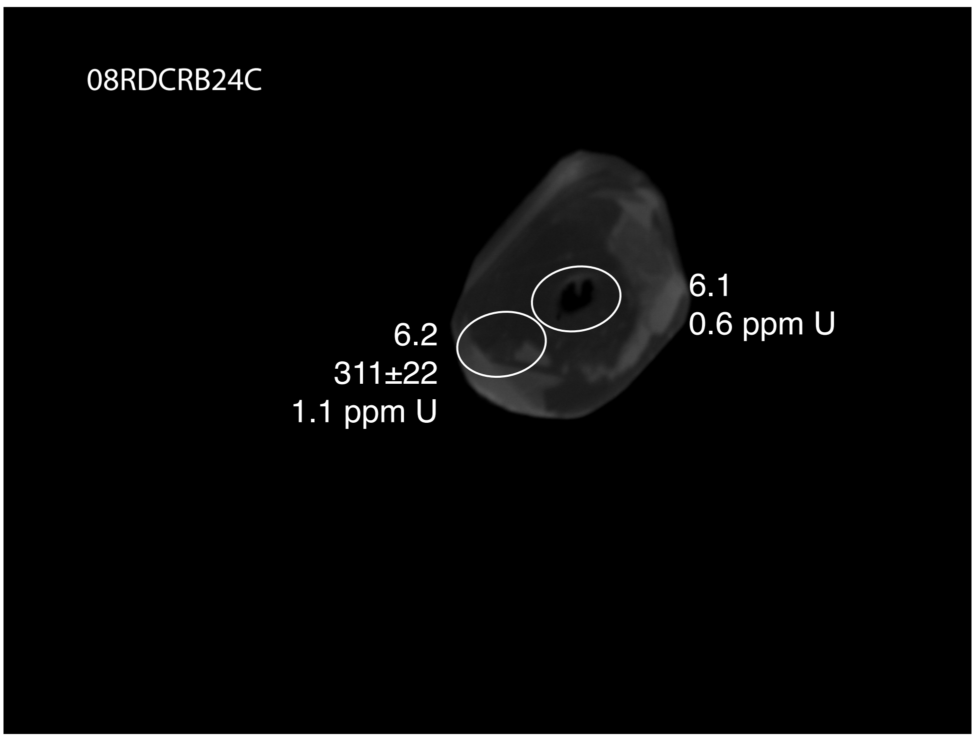
08RDCRB24C
6.1
0.6 ppm U
6.2
311±22
1.1 ppm U

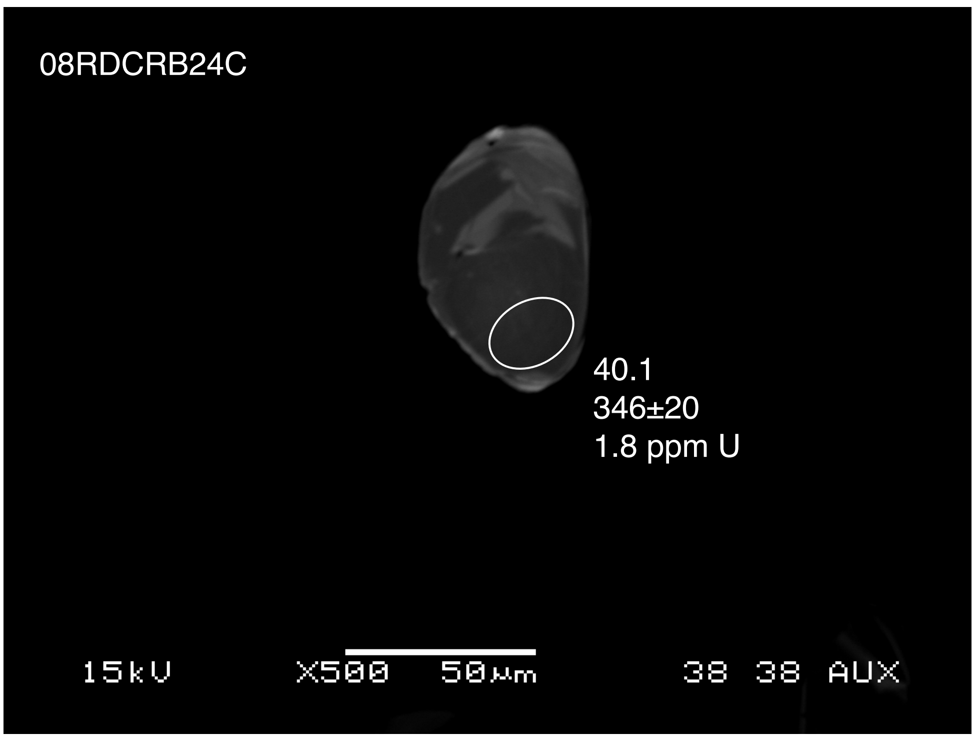
08RDCRB24C
40.1
346±20
1.8 ppm U
15kV
X500
50µm
38 38 AUX

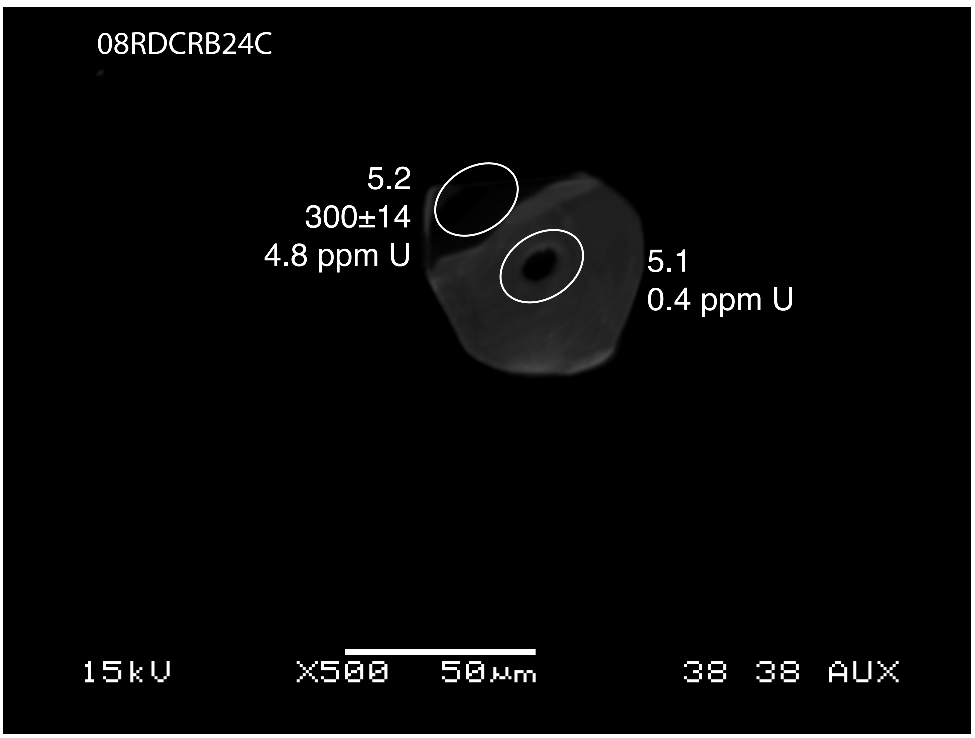
08RDCRB24C
5.2
300±14
4.8 ppm U
5.1
0.4 ppm U
15kV
X500 50μm
38 38 AUX

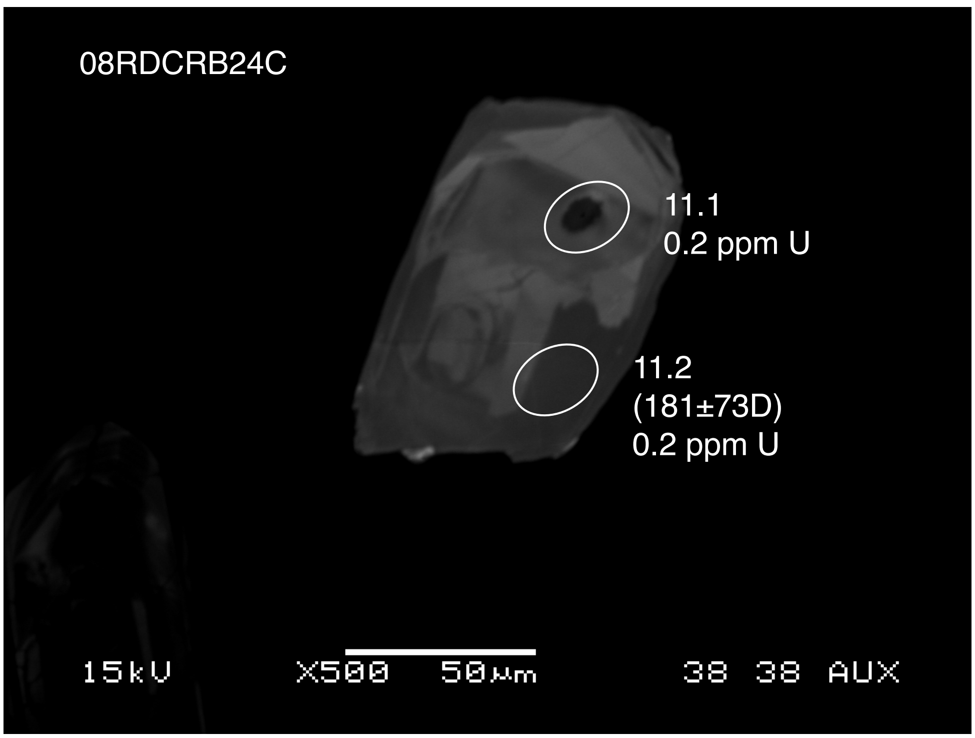

08RDCRB24C
11.1
0.2 ppm U
11.2
(181±73D)
0.2 ppm U
15kV
X500 50µm
38 38 AUX

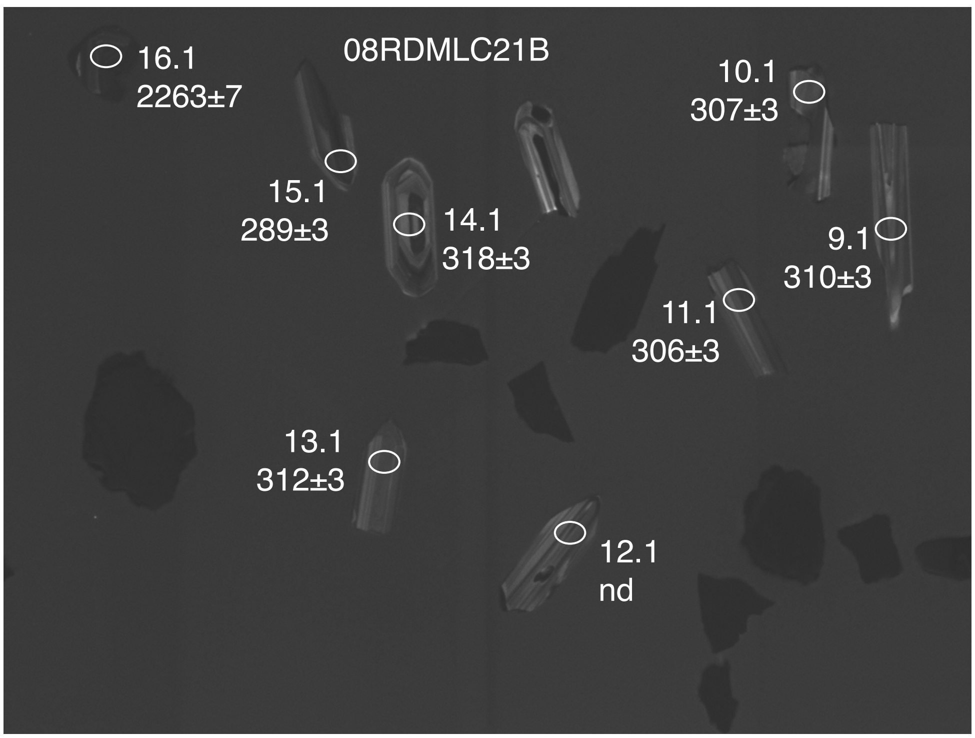
08RDMLC21B
16.1
2263±7
15.1
289±3
14.1
318±3
10.1
307±3
9.1
310±3
11.1
306±3
13.1
312±3
12.1
nd

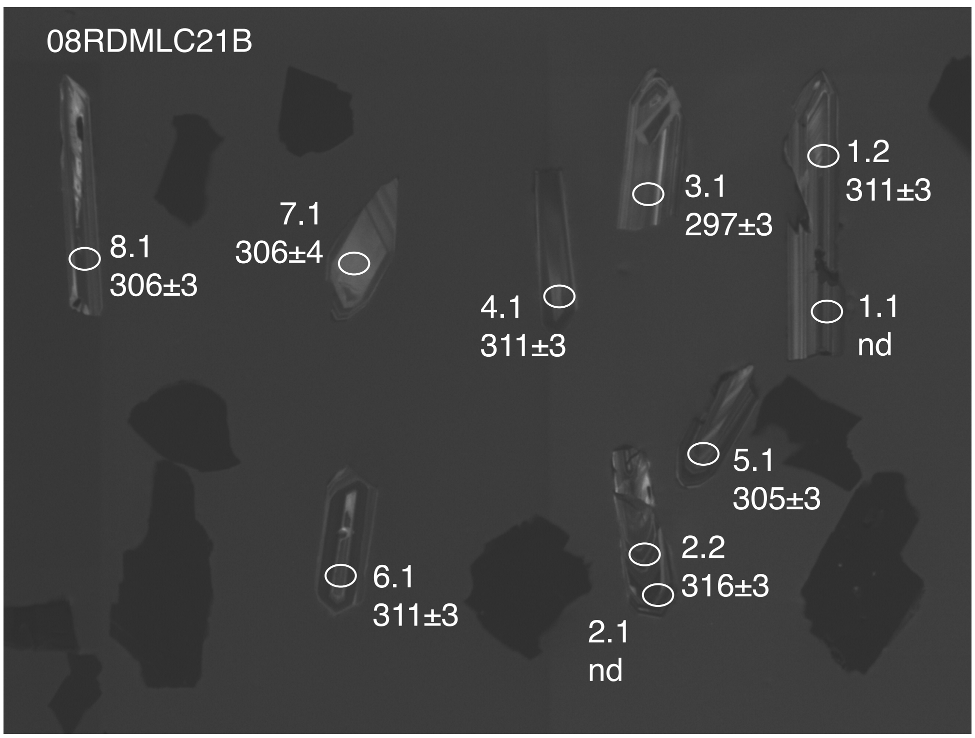
08RDMLC21B
8.1
306±3
7.1
306±4
4.1
311±3
3.1
297±3
1.2
311±3
1.1
nd
5.1
305±3
6.1
311±3
2.2
316±3
2.1
nd

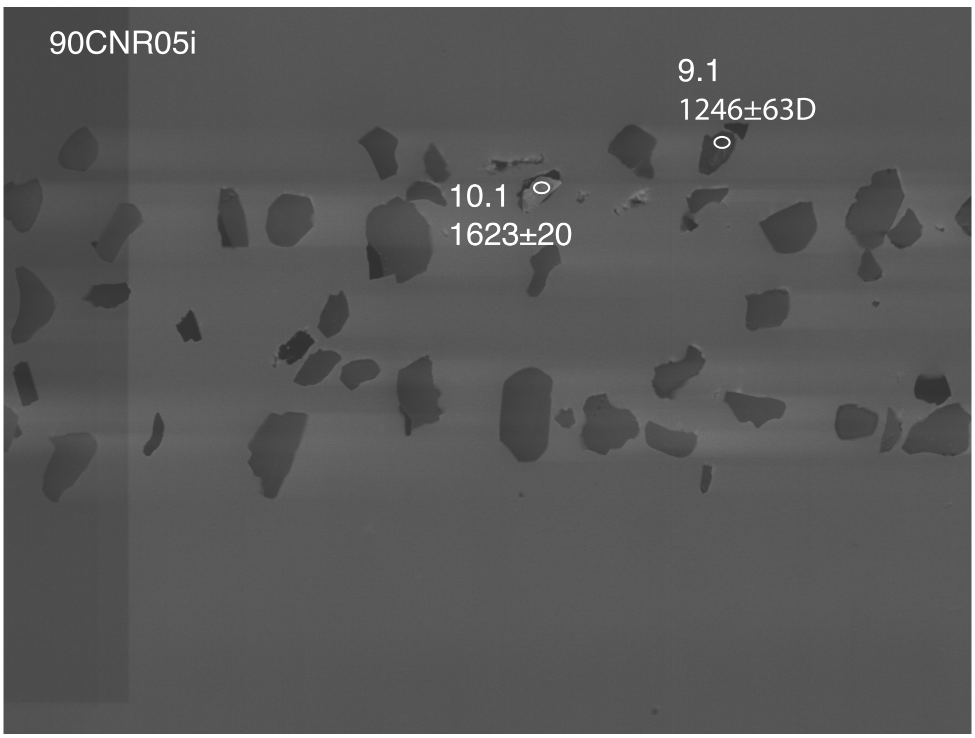
90CNR05i
9.1
1246±63D
10.1
1623±20

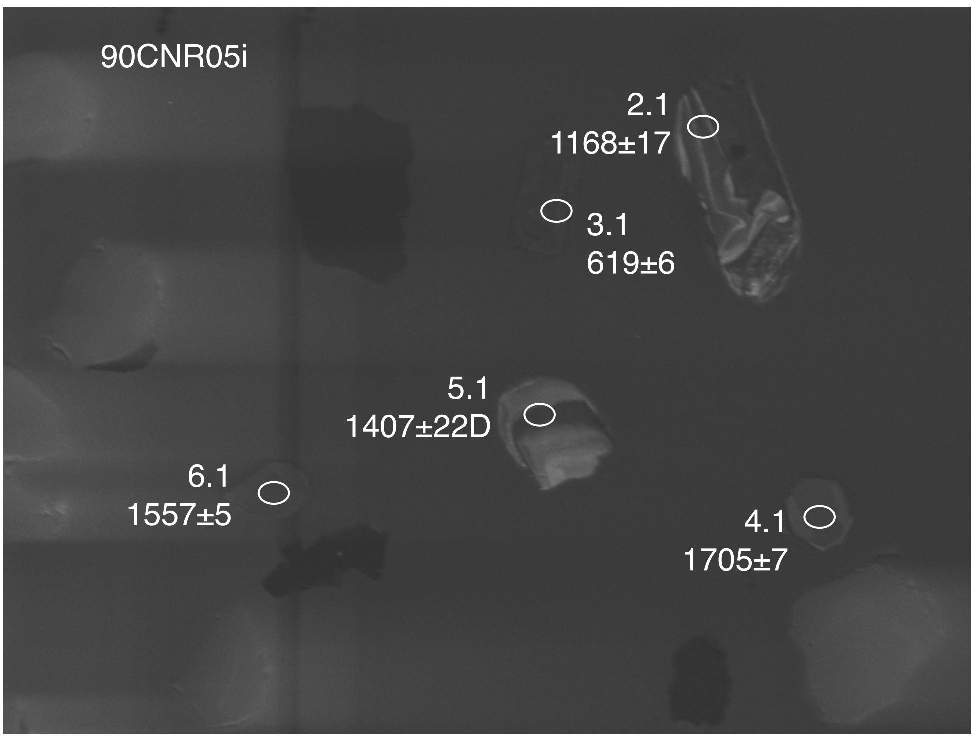
90CNR05i
2.1
1168±17
3.1
619±6
5.1
1407±22D
6.1
1557±5
4.1
1705±7

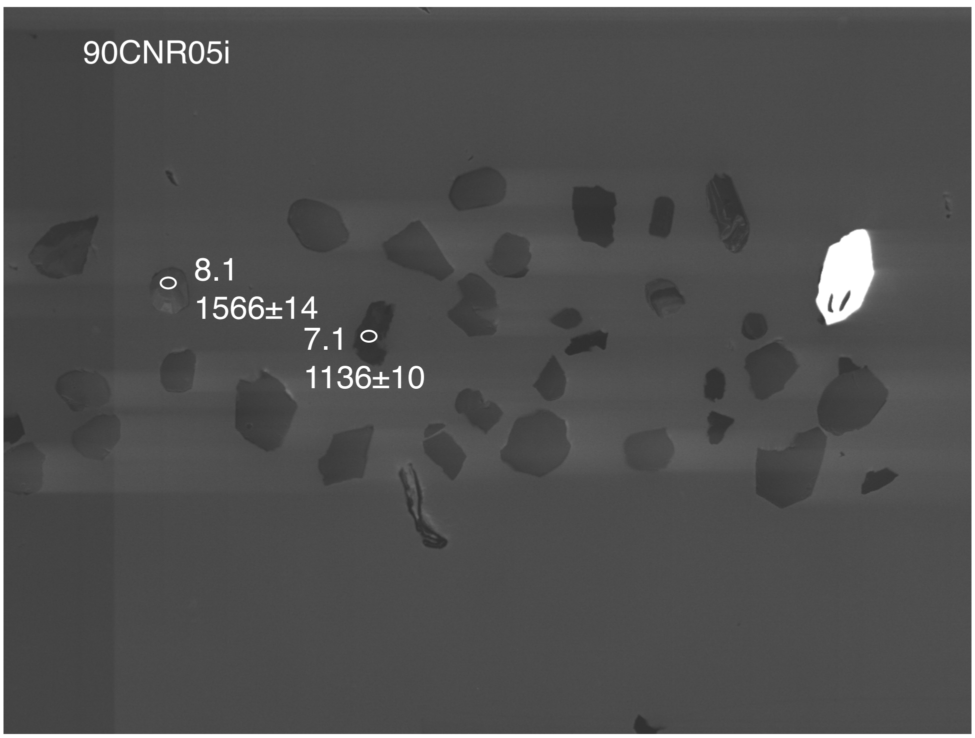

90CNR05i
8.1
1566±14
7.1
1136±10

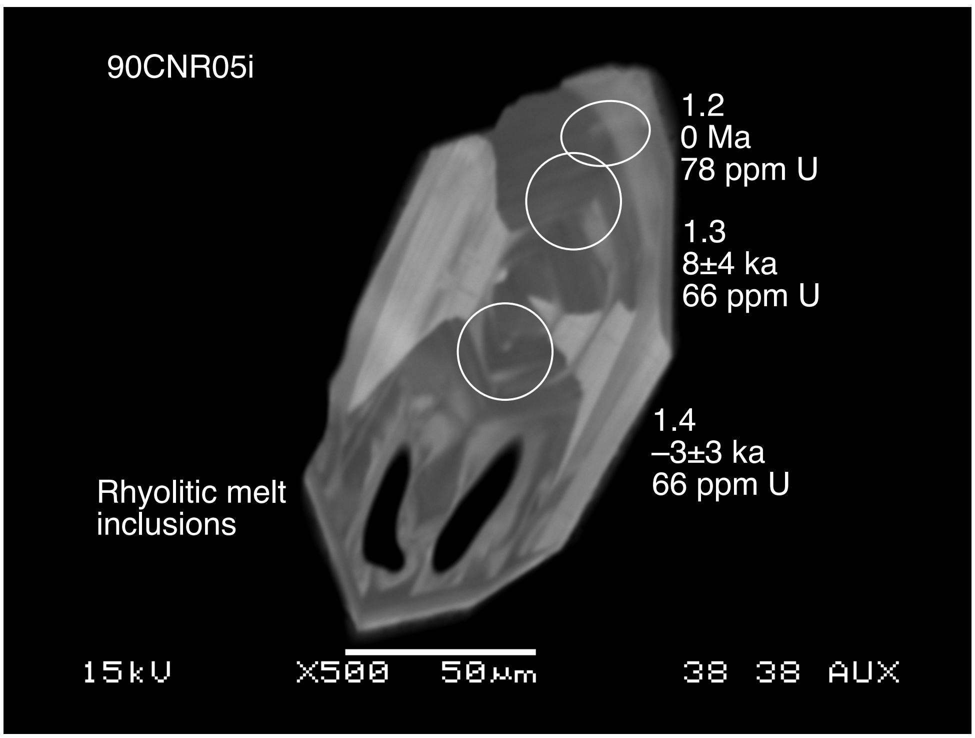

90CNR05i
1.2
0 Ma
78 ppm U
1.3
8±4 ka
66 ppm U
1.4
–3±3 ka
66 ppm U
Rhyolitic melt
inclusions
15kV
X500
50µm
38 38 AUX

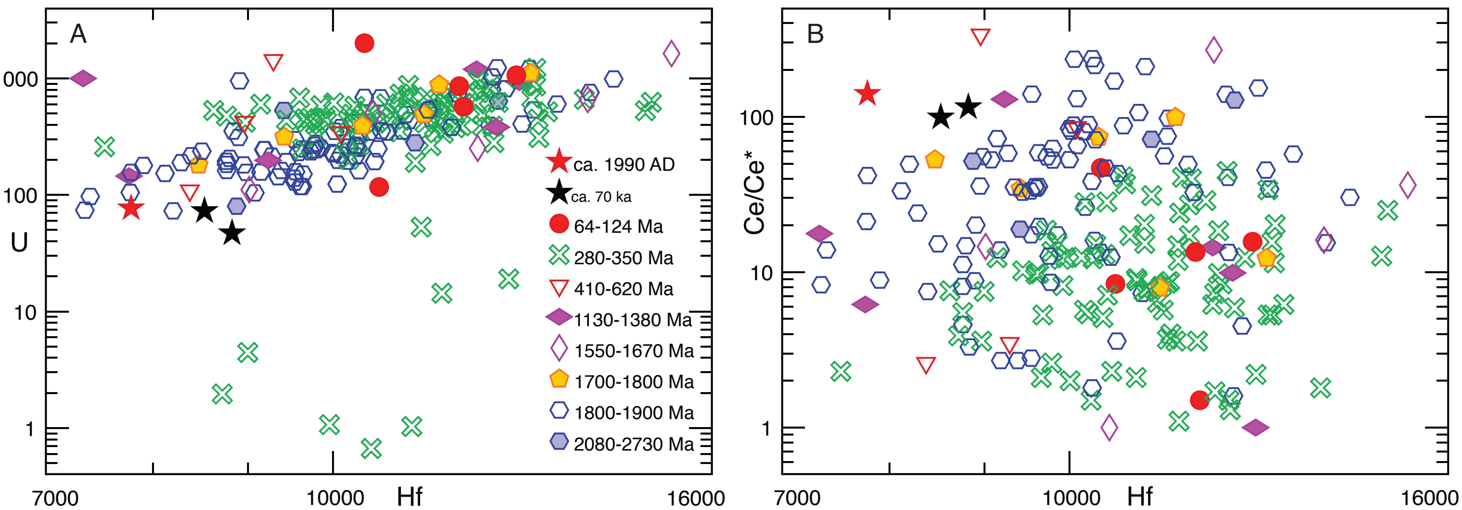

Figure DR5. Concentrations of U and Hf (ppm) and Ce/Ce* ratios in zircon obtained during SHRIMP-RG U–Pb geochronology analyses. Symbols indicate age groups for nominal ages of analysis spots for all six samples plotted together. Note largely separate groups for 1800–1900 Ma and 280–350 Ma points. A: U vs. Hf. B: Ce/Ce* vs. Hf.

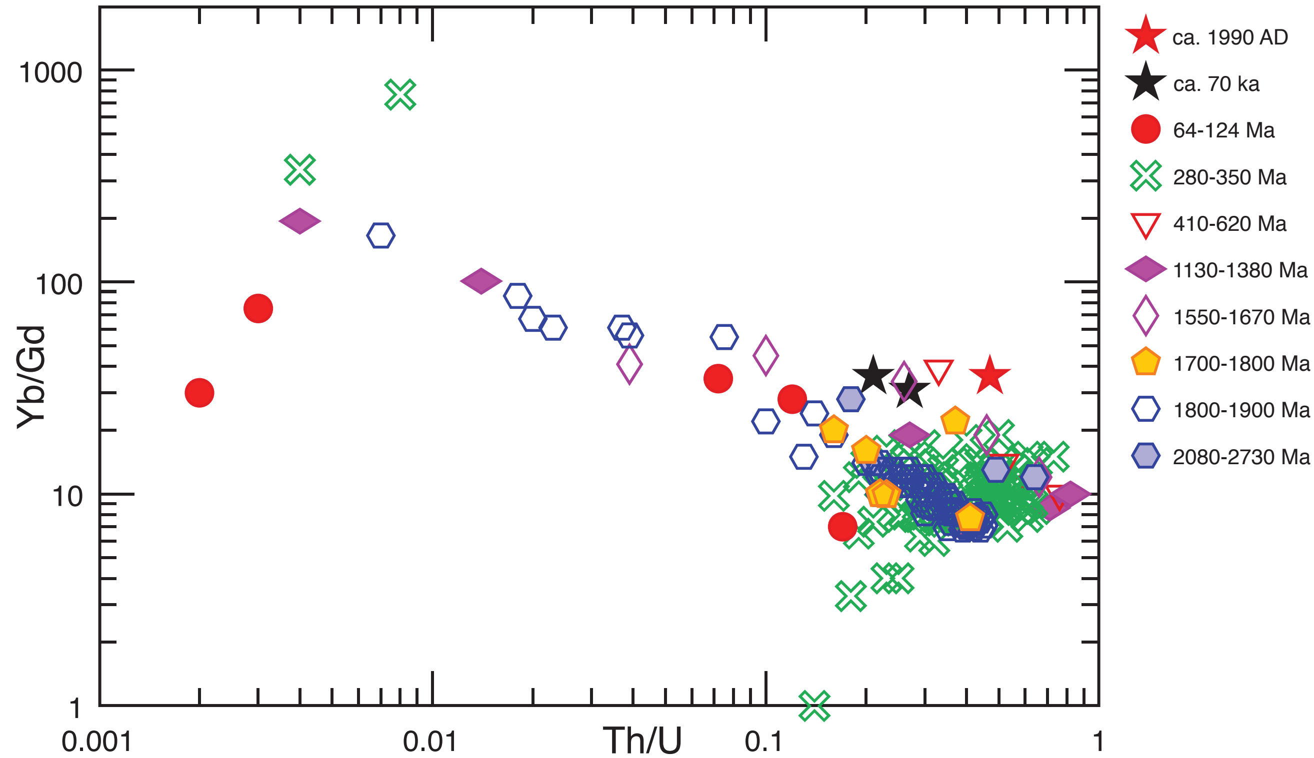

Figure DR6. Concentration ratios Yb/Gd vs. Th/U in zircon obtained during SHRIMP-RG U–Pb geochronology analyses. Symbols indicate age groups for nominal ages of analysis spots for all six samples plotted together. Note coherent trend in 1800–1900 Ma data and clustering of most 280–350 Ma points.

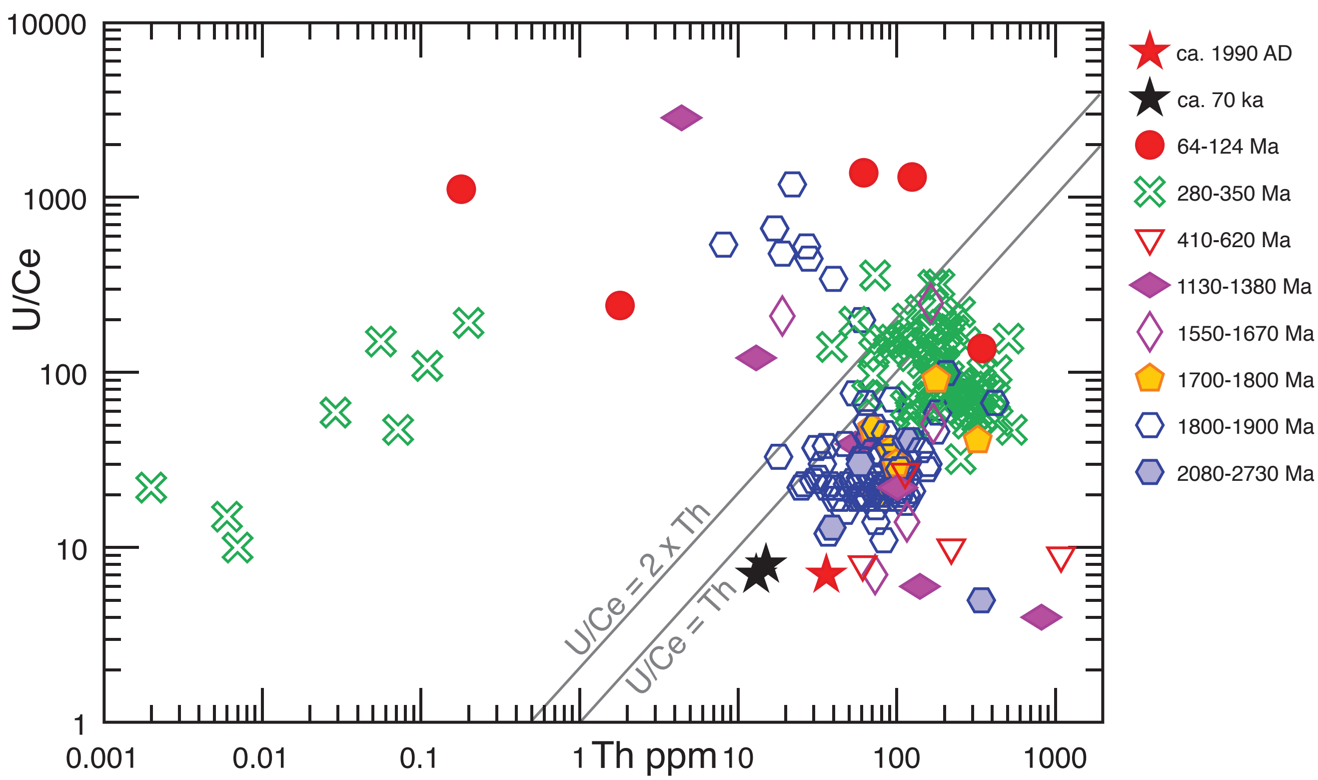

Figure DR7. Concentration ratio U/Ce vs. Th (ppm) in zircon obtained during SHRIMP-RG U–Pb geochronology analyses. Symbols indicate age groups for nominal ages of analysis spots for all six samples plotted together. Gray lines give reference U/Ce:Th ratios. Non-igneous zircon plots at U/Ce>2xTh. Note separation into two clusters for majority of 1800-1900 Ma and 280–350 Ma points. Spot analyzes with U/Ce >2 likely represent zircon that precipitated from aqueous fluid.

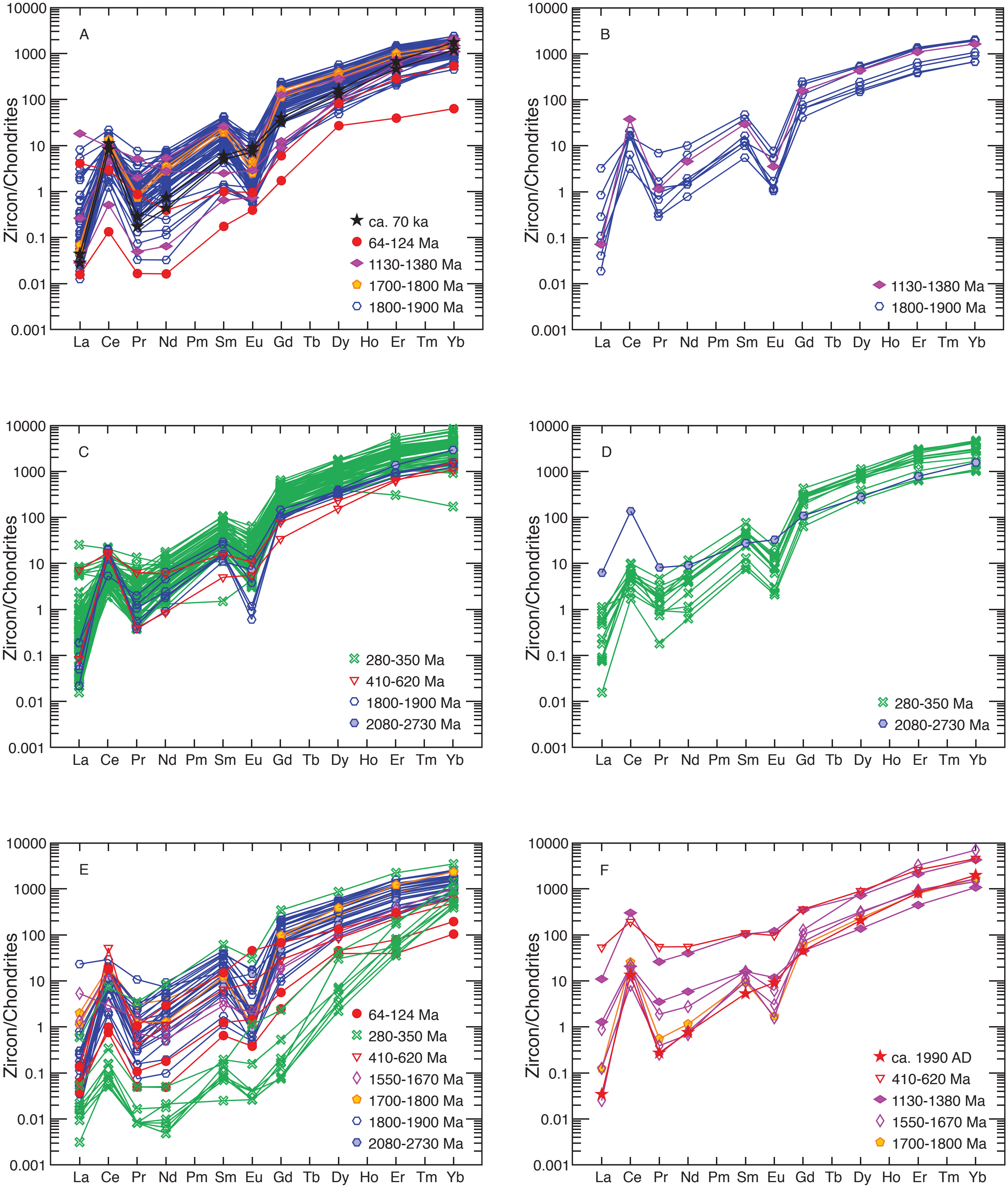

Figure DR8. Concentrations of REE in zircon obtained during SHRIMP-RG U–Pb geochronology analyses normalized to those in chondritic meteorites (Korotev, 1996). Values for Pr calculated on the basis of those for La and Nd. Symbols indicate age groups for nominal ages of analysis spots. A: Crystal mush 19B. B: Gabbro 22. C: Gabbro 24B. D: Gabbro 21B. E: Gabbro 24C. F: Gabbro 5i.